International Communications in Heat and Mass Transfer 161 (2025) 108447

Contents lists available at ScienceDirect

International Communications in Heat and Mass Transfer

journal homepage: www.elsevier.com/locate/ichmt

Geometrical optimization of an isothermal double Y-shaped cavity employing differential evolution algorithm with a constructal approach

Gill Velleda Gonzales [a,b], Cesare Biserni [c,*], Luiz Alberto Oliveira Rocha [a], Emanuel da Silva Diaz Estrada [a], Liércio André Isoldi [a], Antônio José da Silva Neto [d], Elizaldo Domingues dos Santos [a]

[a] Graduate Program of Computational Modeling, Federal University of Rio Grande - FURG, CEP 96201-900 Rio Grande, RS, Brazil
[b] Federal Institute of Education, Science and Technology Sul-Rio-Grandense, Campus Pelotas, CEP 96015-360 Pelotas, RS, Brazil
[c] Department of Industrial Engineering (DIN), Alma Mater Studiorum - University of Bologna, Viale Risorgimento 2, 40136 Bologna, Italy
[d] Polytechnic Institute, Rio de Janeiro State University, CEP 28625-570 Nova Friburgo, RJ, Brazil

ARTICLE INFO

Keywords:
Constructal design
Differential evolution
Optimization
Double Y-shaped cavity
Heat generating walls

ABSTRACT

This numerical work deals with constructal design (CD) to investigate a complex isothermal double-Y-cavity geometry inserted for chilling a rectangular heat-generating solid body. The purpose is to minimize the dimensionless maximum temperature excess in the solid domain for the geometry with four constraints and seven degrees of freedom (DOF), giving more freedom compared with previous cavities. The optimization process is performed with exhaustive search (ES) and differential evolution (DE) from the fourth DOF onward to reproduce the effect of the analyzed DOFs on the performance indicator and design. For square solids, the optimal geometries were obtained when the branches of the investigated cavity were stretched, covering the solid body and distributing the hot regions more homogeneously, i.e., following the optimal distribution of imperfections principle. For square solids, the performance of the present cavity was 82 %, 74 %, 70 %, 45 %, 35 %, and 25 % superior to I-, T-, Y-, X-, double T-, and H-cavities, and 1.0 % inferior to ψ configuration. For low and high height/length (H/L) ratios of the solid domain, the optimal configurations were obtained when the double Y-shaped cavity changed to double T and I configurations, respectively, showing the impact of the constraints on the design of the cavity.

1. Introduction

Constructal theory indicates that the designs emerging in flow systems, including those noticed in nature, do not result from chance [1,2], resulting from an evolutionary process and following the constructal law of evolutionary design [1–4]. This physical principle states that for a finite-size flow system to remain alive over time, its design must freely evolve to facilitate access to the internal currents in the system [1–5]. As a universal design principle, constructal law has contributed to predicting the design and rhythm in several fields, such as biology, medicine, and social dynamics [5,6–8]. The method to employ the constructal law in the determination of the design of flow systems is the constructal design (CD). Constructal design is based on constraints (geometrical, physical, technological, and other) and goals (performance indicators). The design (expressed by the degrees of freedom of the geometry) is varied to comprehend its influence on the performance indicators that are maximized and/or minimized [9–11]. The effectiveness of the method in investigating the design of several engineering applications such as cooling cavities, fins and porous fins, finned heat sinks, convective channels, "flow of stresses" in structural engineering, cooling of electronic packaging, heat exchangers, and renewable energy has been successfully demonstrated in the works of literature [11–24].

One of the most common designs seen in the flow systems is the tree-like pattern, as can be noticed, for example, in trees, rivers, human lungs, animal design, flight routes, or streets in the cities [5]. This kind of configuration is characteristic of point-volume (or volume-point) flows with low resistance pathways placed over a background of high resistance and for a flow system with enough flow intensity [12,25–28]. Studies of cavities and high-conductive pathways have been widely investigated in the literature [26,28–34] due to the simplicity of the physical problem and the possibility of solving several cases and studying the generation of complex configurations for the cavities and conductive pathways. Recently, important contributions have been also

* Corresponding author.
E-mail address: cesare.biserni@unibo.it (C. Biserni).

https://doi.org/10.1016/j.icheatmasstransfer.2024.108447

Available online 6 December 2024

Nomenclature

A	Area, m^2
CR	Crossover rate parameter
F	Mutation function amplification factor
G	Actual generation of optimization method
H	Height of the solid wall, m
H_0	Height of the cavity trunk, m
H_1	Thickness of the inferior cavity branches, m
H_2	Thickness of the superior cavity branches, m
k	Thermal conductivity of the solid body, $W \bullet m^{-1} \bullet K^{-1}$
L	Length of the solid body, m
L_0	Thickness of the cavity trunk, m
L_1	Length of the inferior cavity branches, m
L_2	Length of the superior cavity branches, m
NP	Population size (number of solutions)
NG	Number of generations
OF	Objective function
q	Heat transfer rate, W
q'''	Heat transfer rate per unit volume, $W \cdot m^{-3}$
T	Temperature, K
u	Solution of the next generation of the optimization method
W	Width, m
v	Trial vector with candidate solution of optimization method
x, y	Cartesian coordinates, m

Greek symbol

ΔE	Difference between the cost of the objective function for the new and best solutions
θ	Dimensionless excess of temperature
φ	Cavity fraction area
α	Angle of the inferior cavity branches, degrees (°)
β	Angle of the superior cavity branches, degrees (°)

Abbreviations

CD	Constructal Design
CR	Crossover rate parameter of differential evolution algorithm
DOF	Degrees of Freedom
DE	Differential Evolution
ES	Exhaustive Search
F	Amplification factor parameter of differential evolution algorithm
GA	Genetic Algorithm
SA	Simulated Annealing

Superscripts

()	dimensionless variables

Subscripts

c	Cavity
max	Maximum
min	Minimum
m	Once minimized
*n*m	*n* times minimized
*n*o	*n* times optimized
r	Random index for operations with population solutions in the mutation function
0, 1, 2	Variable indexes of height and length for the trunk, inferior and superior branches, respectively

made to the construction of branched pathways and using hybrid conductive pathways and fluid flow cooling of solids with heat generation and stacked chips [35–36]. Moreover, since the design of the cavity problem can ideally represent the flow systems abundant in nature, some meaningful analogies can be performed between the cavity problem and real flow systems, e.g., comprehension of the influence of the neighborhood and constraint conditions on the design and purpose of the flow system [28–29]. Also, recommendations in cooling cavities can supply theoretical guidelines to improve performance in cooling systems of compact and miniaturized packages of electronics [28–29].

The pioneering work of Bejan [1] presented an investigation about the generation and growth of the design of high conductive pathways mounted in heat-generating rectangular solid walls from the elemental configuration (I-shaped pathway) towards a treelike network using the previous step to define the new level of construction. Into the cavities realm, Biserni et al. [28] investigated the design of elemental (I-shaped) and first-construct (T-shaped) cavities considering the influence of the first construct degree of freedom (bifurcation of T) on the configuration of the elemental trunk, i.e., the construct did not use a memory strategy for the second level of construction. This work showed that the first construct (T-shaped cavity) performed better than the elemental configuration for equivalent thermal conditions and problem constraints. Results also indicated that the increase of the cavity intrusion into the solid domain contributed to an augmentation in the performance of the solid/cavity system. Over the years, several studies were performed to investigate other configurations of cavities intruded into solid walls considering only one sink point, for example, T-, Y-, H-, X-, ψ- and tree-shaped cavities [13,14,29,30,37–39]. In general, the exhaustive search (ES) was associated with constructal design (CD) to investigate the construction that minimizes the maximum excess of temperature (θ_{max}). However, other performance indicators, such as entropy generation have also been employed [31]. The main purpose of those studies was to investigate how the insertion of new construction levels affected the design and performance of the system. Among the several investigated configurations, the H-shaped cavity studied by Biserni et al. [13] demonstrated that the best geometry for the second construct design performs much better than the previous constructions, i.e., the I- and T-shaped configurations. Similar performance was obtained later for cavities with one heat sink under the same thermal conditions for the ψ-, double-T-cavity, and tree-shaped configurations [14,26,30].

In general, it was noticed in the literature results that for isothermal cavities inserted into heat-generating solid walls, the increase of the geometric complexity (with an investigation of more DOFs) led to a more homogeneous distribution of hot spots and an increase of the thermal performance, i.e., following the optimal distribution of imperfections principle [28–41]. Other important works evaluated the impact of the coefficient of convection heat transfer (h) imposed in the cavity surfaces on the performance indicator of the system for different cavity configurations (I, T, and Y), simulating the influence of neighborhood on the design [42–44]. These studies indicated that the optimal designs for cavities with low magnitudes of h had simple designs and few intrusions into the solid domain. This behavior is dissimilar to that observed for high magnitudes of h, where the cavity was more complex and had a deeper intrusion in the solid domain.

One limitation for the investigation of complex configurations, study of different parameters (e.g., boundary conditions), and adequate reproduction of the influence of the degrees of freedom (DOFs) over the performance parameters is the prohibitive number of required simulations (cases) for application of ES, which is the benchmark solution in the optimization of this problem [26]. For instance, a problem with seven DOFs, as studied in the present work, would require at least 10^7

simulations considering a discretization of search space with ten simulations per DOF. In this sense, recent works have attempted to associate computational intelligence optimization methods with CD to investigate more parameters as different fractions and occupation areas of the cavity [26,44–48]. This strategy has also been used for the geometric optimization of high-conductive pathways and compound channels [17,49]. The main concern in this kind of investigation is not seeking global optimal configurations but the comprehension of the behavior of the design and system performance, represented by the effect of DOFs on the performance indicator and other optimized DOFs in different optimization levels.

Examples related to the association between constructal design and computational intelligence have grown in the literature. For example, Lorenzini et al. [44] applied GA to investigate the impact of the coefficient h on the performance of the Y-shaped cavity and optimal configuration considering four DOFs. Lorenzini et al. [45] also studied the CD method combined with the genetic algorithm (GA) metaheuristic to evaluate a cavity in the form of Y. Later, Gonzales et al. [46] associated the simulated annealing (SA) heuristic with CD to investigate the geometry of a cavity in the form of Y with four DOFs. The main concern was to increase the reliability of the prediction of the behavior of the DOFs over θ_{max} at different optimization levels. Gonzales et al. [47] compared the SA and Luus-Jaakola (LJ) heuristic algorithms applied to the optimization of a few DOFs of a cavity in the form of double T. SA algorithm was better succeeded than LJ in the prediction of the global optimal configurations (for the investigated DOFs) and for determination of the influence of DOFs over thermal objective function. Based on the study of Ref. [47], Gonzales et al. [26] performed the complete optimization of the cavity in the form of double T associating CD and SA for optimization of five DOFs, also investigating the influence of cavity fraction area on the thermal performance and design of the cavity. Gonzales et al. [48] performed the association between differential evolution (DE) and CD to optimize a double T-shaped cavity. DE algorithm was superior to the SA method for optimizing and investigating the geometry. Moreover, different parameters of DE were analyzed and compared, seeking to predict the outcome of the geometry on the θ_{max} for the cavity in the form of double T. Considering the investigated parameters, the best results were obtained for the operator of mutation *rand/1/bin*, crossover rate (CR) equal to 0.7, and amplification factor (F) of 1.5. Recently, Gonzales et al. [32] investigated the use of DE for partial optimization of four DOFs of the double Y-shaped cavity. The purpose was to study the sixteen combinations of DE algorithms statistically, considering different mutation parameters, crossover rate (CR), and amplification factor (F). The goal was to identify the parameters that increase the efficiency of the meta-heuristic to obtain the optimal configurations and conduct adequate predictions about the effect of investigated DOFs on the performance indicator. It is also worth mentioning that some recent advances in applying machine learning and artificial intelligence have been obtained for a better exploration of the results and optimization in cavity flows [50,51].

In the present study, an isothermal cavity with complex double Y-shaped geometry is optimized entirely using the association between constructal design (CD), exhaustive search (ES), and differential evolution (DE) methods. More precisely, seven DOFs are optimized for varied fraction areas of the cavity. The focus here is dissimilar to that performed in Gonzales et al. [32], where the concern was restricted to defining the best DE parameters for a few DOF investigations. Here, the main contribution is to analyze the influence of a new complex cavity design for all seven DOFs over the thermal performance and optimal DOFs, using a new hybrid approach between the ES and DE algorithm as a tool for applying CD in the complex system. The present configuration represents an evolution of the double-T-cavity configuration studied in Ref. [22] and the tree-shaped cavity with two branches ($N = 2$) presented in Ref. [14], since it is given freedom to the bifurcated branches to rotate. To the best of the authors' knowledge, a complex configuration that can ideally represent a tree-shaped configuration with seven DOFs

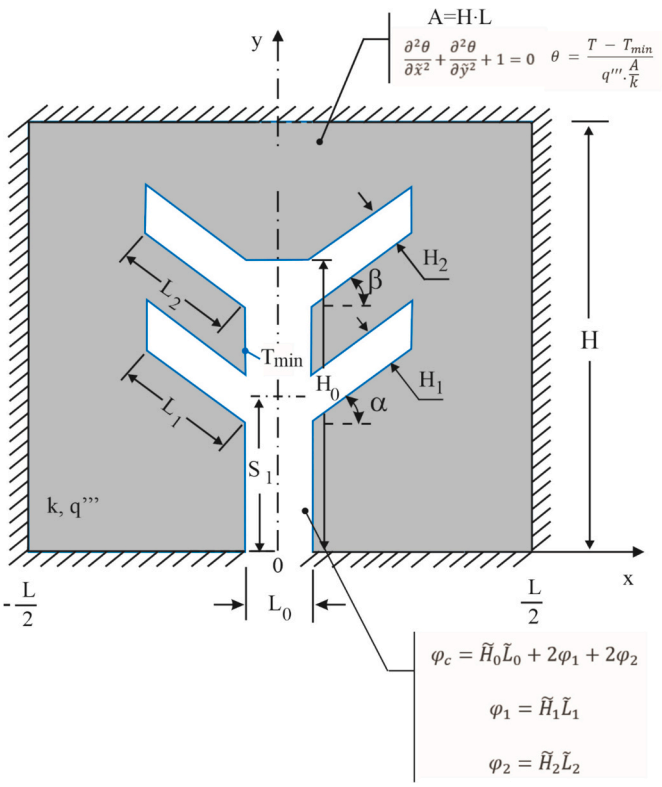

Fig. 1. Computational domain of the cavity in form of double Y intruded into a rectangular heat generating solid wall.

using CD, ES, and DE to understand the influence of the design over thermal performance has not been previously investigated in the literature. Moreover, the analysis performed here using solely ES would be unfeasible since it would require more than forty hundred million simulations.

2. Mathematical and numerical modeling

2.1. Physical and geometrical problem statement

It is considered here a two-dimensional solid body subjected to constant heat generation per unit volume, q''' (Wm^{-3}), cooled by the insertion of an isothermal double Y-shaped cavity, as illustrated in Fig. 1. Moreover, the external surfaces of the solid domain (dashed in Fig. 1) are adiabatic, in such a way the heat generation in the solid can be removed only by the cavity at a minimum temperature (T_{min}). The problem is subjected to the following simplifying hypothesis, as performed previously in the works of Refs. [13, 28–30, 32, 37]:

- the solid domain has constant thermal conductivity (k);
- the cavity surfaces are isothermal (simulating fluid flow with constant high coefficient h, e.g., phase of change flow);
- the thermal field is in the steady state;
- the magnitude of q''' is uniform and constant;
- the problem is modeled as two-dimensional.

The fluid flow in the cavity is not modeled, and the convection heat transfer is treated as a boundary condition in the solution of conduction heat transfer in the solid domain. Therefore, the modeling of the temperature as a function of spatial coordinates, $T = f(x, y)$, in the solid domain is given by the following simplified heat diffusion equation:

$$\frac{\partial^2 T}{\partial x^2}+\frac{\partial^2 T}{\partial y^2}+\frac{q'''}{k}=0 \tag{1}$$

where x and y are the coordinates in the space (m), k is the thermal conductivity ($W \bullet m^{-1} \bullet K^{-1}$), q''' is the heat generated in the solid wall ($W \bullet m^{-3}$), and T is the temperature (K).

The goal of the investigation is to reach the optimal DOFs of the cavity (H/L, H_0/L_0, S_1/H_0, α, β, H_1/L_1, and H_2/L_2) that minimizes the maximum excess of temperature (T_{max} - T_{min})/($q'''A$). For the application of the CD, the problem has two constraints, the total domain and cavity areas, which are given, respectively, by:

$$A = HL \tag{2}$$

$$A_c = H_0 L_0 + 2H_1 L_1 + 2H_2 L_2 \tag{3}$$

The total area and the cavity area can be represented in their dimensionless form by the ratio between the cavity and total domain areas, as given by:

$$\varphi_c = \frac{A_c}{A} \tag{4}$$

The heat diffusion equation can also be modeled in its dimensionless form by the following expression:

$$\frac{\partial^2 \theta}{\partial \tilde{x}^2} + \frac{\partial^2 \theta}{\partial \tilde{y}^2} + 1 = 0 \tag{5}$$

Here, the dimensionless temperature and spatial coordinates are given, respectively, by:

$$\theta = \frac{T - T_{min}}{q''' \cdot \frac{A}{k}} \tag{6}$$

$$\tilde{x}, \tilde{y}, \tilde{H}, \tilde{L}, \tilde{H}_0, \tilde{L}_0, \tilde{H}_1, \tilde{L}_1, \tilde{H}_2, \tilde{L}_2, \tilde{S}_1 = \frac{x, y, H, L, H_0, L_0, H_1, L_1, H_2, L_2, S_1}{A^{\frac{1}{2}}} \tag{7}$$

The equations that represent the adiabatic boundary conditions in the external surfaces and the boundary condition of minimum temperature ($\theta = \theta_{min}$) at the cavity surfaces are described in the following equations, and the boundary conditions, also are illustrated in Fig. 1.

$$\frac{\partial \theta}{\partial \tilde{x}} = 0 \; at \; \tilde{x} = -\frac{\tilde{L}}{2} \; or \; \frac{\tilde{L}}{2} \; and \; 0 \le \tilde{y} \le \tilde{H} \tag{8}$$

$$\frac{\partial \theta}{\partial \tilde{y}} = 0 \; at \; \tilde{y} = 0 \; and - \frac{\tilde{L}}{2} \le \tilde{x} \le -\frac{\tilde{L}_0}{2} \; or \; \frac{\tilde{L}_0}{2} \le \tilde{x} \le \frac{\tilde{L}}{2} \tag{9}$$

$$\frac{\partial \theta}{\partial \tilde{y}} = 0 \; at \; \tilde{y} = \tilde{H} \; and - \frac{\tilde{L}}{2} \le \tilde{x} \le \frac{\tilde{L}}{2} \tag{10}$$

$$\theta = \theta_{min} \; in \; 0 \le \tilde{y} \le \tilde{S}_1 - \frac{\tilde{H}_1}{2sin(90^\circ - \alpha)} \; and \; \tilde{x} = -\frac{\tilde{L}_0}{2} \; or \; \tilde{x} = \frac{\tilde{L}_0}{2} \tag{11}$$

$$\theta = \theta_{min} \; in \; \tilde{S}_1 - \frac{\tilde{H}_1}{2sin(90^\circ - \alpha)} \le \tilde{y} \le \tilde{L}_1 sin\alpha + \tilde{S}_1 - \frac{\tilde{H}_1}{2sin(90^\circ - \alpha)}$$

$$and - \frac{\tilde{L}_0}{2} - \tilde{L}_1 cos\alpha \le \tilde{x} \le -\frac{\tilde{L}_0}{2} \; or \; \frac{\tilde{L}_0}{2} \le \tilde{x} \le \frac{\tilde{L}_0}{2} + \tilde{L}_1 cos\alpha \tag{12}$$

$$\theta = \theta_{min} \; in \; \tilde{x} = -\frac{\tilde{L}_0}{2} - \tilde{L}_1 cos\alpha \; or \; \tilde{x} = \frac{\tilde{L}_0}{2} + \tilde{L}_1 cos\alpha$$

$$and \; \tilde{L}_1 sin\alpha + \tilde{S}_1 - \frac{\tilde{H}_1}{2sin(90^\circ - \alpha)} \le \tilde{y} \le \tilde{L}_1 sin\alpha + \tilde{S}_1 + \frac{\tilde{H}_1}{2sin(90^\circ - \alpha)} \tag{13}$$

$$\theta = \theta_{min} \; in - \frac{\tilde{L}_0}{2} - \tilde{L}_1 cos\alpha \le \tilde{x} \le -\frac{\tilde{L}_0}{2} \; or \; \frac{\tilde{L}_0}{2} \le \tilde{x} \le \frac{\tilde{L}_0}{2} + \tilde{L}_1 cos\alpha$$

$$and \; \tilde{S}_1 + \frac{\tilde{H}_1}{2sin(90^\circ - \alpha)} \le \tilde{y} \le \tilde{L}_1 sin\alpha + \tilde{S}_1 + \frac{\tilde{H}_1}{2sin(90^\circ - \alpha)} \tag{14}$$

$$\theta = \theta_{min} \; in \; \tilde{S}_1 + \frac{\tilde{H}_1}{2sin(90^\circ - \alpha)} \le \tilde{y} \le \tilde{H}_0 - \frac{\tilde{H}_2}{sin(90^\circ - \beta)}$$

$$and \; \tilde{x} = -\frac{\tilde{L}_0}{2} \; or \; \tilde{x} = \frac{\tilde{L}_0}{2} \tag{15}$$

$$\theta = \theta_{min} \; in - \frac{\tilde{L}_0}{2} - \tilde{L}_2 cos\beta \le \tilde{x} \le -\frac{\tilde{L}_0}{2} \; or \; \frac{\tilde{L}_0}{2} \le \tilde{x} \le \frac{\tilde{L}_0}{2} + \tilde{L}_2 cos\beta$$

$$and \; \tilde{H}_0 - \frac{\tilde{H}_2}{sin(90^\circ - \beta)} \le \tilde{y} \le \tilde{H}_0 - \frac{\tilde{H}_2}{sin(90^\circ - \beta)} + \tilde{L}_2 sin\beta \tag{16}$$

$$\theta = \theta_{min} \; in \; \tilde{x} = -\frac{\tilde{L}_0}{2} - \tilde{L}_2 cos\beta \; or \; \tilde{x} = \frac{\tilde{L}_0}{2} + \tilde{L}_2 cos\beta$$

$$and \; \tilde{H}_0 - \frac{\tilde{H}_2}{sin(90^\circ - \beta)} + \tilde{L}_2 sin\beta \le \tilde{y} \le \tilde{H}_0 + \tilde{L}_2 sin\beta \tag{17}$$

$$\theta = \theta_{min} \; in \; \tilde{H}_0 \le \tilde{y} \le \tilde{H}_0 + \tilde{L}_2 sin\beta$$

$$and - \frac{\tilde{L}_0}{2} - \tilde{L}_2 cos\beta \le \tilde{x} \le -\frac{\tilde{L}_0}{2} \; or \; \frac{\tilde{L}_0}{2} \le \tilde{x} \le \frac{\tilde{L}_0}{2} + \tilde{L}_2 cos\beta \tag{18}$$

$$\theta = \theta_{min} \; in \; \tilde{y} = \tilde{H}_0 \; and - \frac{\tilde{L}_0}{2} \le \tilde{x} \le \frac{\tilde{L}_0}{2} \tag{19}$$

The constraint areas, Eqs. (2)–(3) are also represented in the dimensionless form by:

$$\tilde{H}\tilde{L} = 1 \tag{20}$$

$$\varphi_c = \tilde{H}_0 \tilde{L}_0 + 2\varphi_1 + 2\varphi_2 \tag{21}$$

$$\varphi_1 = \tilde{H}_1 \tilde{L}_1 \tag{22}$$

$$\varphi_2 = \tilde{H}_2 \tilde{L}_2 \tag{23}$$

The performance indicator to be minimized is the dimensionless maximum excess of temperature, which is given by:

$$\theta_{max} = \frac{T_{max} - T_{min}}{q''' \cdot \frac{A}{k}} \tag{24}$$

To define the $(\theta_{max})_{7m}$, it is necessary to optimize the seven DOFs submitted to the cavity area constraints and the total area of the solid. Here, the subscript "*Nm*" represents the performance indicator (θ) *N* times minimized, and the subscript "*No*" is related to the DOF *N* times optimized. For example, $(\theta_{max})_{2m}$ and $(\beta)_{2o}$ represent the θ and β two times minimized and optimized, respectively. The procedure of geometrical optimization is detailed in section 3.

2.2. Numerical method

The value of the θ_{max} in Eq. (24) was reached by the prediction of the temperature fields with the Finite Element Method (FEM) that solves Eq. (5) for the computational domain of every case. The FEM was implemented in the PDE *toolbox* (Partial Differential Equation Toolbox) from the MATLAB® software [52]. This software package has been used in several works about cooled cavities in the studies of literature [26,28–32,37–49]. It is assumed as an initial guess for the problem solution that all the domain is at θ_{min} for the first iteration step.

The mesh employed in the simulations is determined after making an independent mesh investigation, which consists of the simulation of the same case with different meshes seeking to identify the asymptotic re-

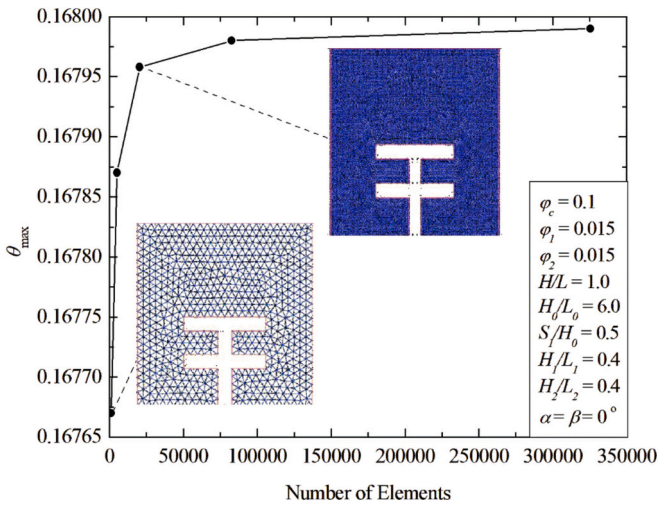

Fig. 2. Grid independence study performed for one specific case of the present work.

Table 1
Verification of the θ_{max} obtained with the present computational method for the constraints and DOFs ($\varphi_c = 0.1$; $\varphi_1 = 0.02$; $\varphi_2 = 0.02$; $H/L = 1$; $H_0/L_0 = 20$; $S_1/H_0 = 0.45$; $H_1/L_1 = 14$; $H_2/L_2 = 0.14$; $\alpha = \beta = 0°$) compared with results of literature [26,28,39].

Reference	θ_{max}
Present Work	0.0756
Biserni et al. [28]	0.0755
Lorenzini et al. [39]	0.0762
Gonzales et al. [26]	0.0756

gion where the number of grid elements has little influence on the computational solution. The mesh independent study was based on the work of Ref. [32], and the employed criterion to find the correct mesh is determined by:

$$\left|\frac{(\theta^{i}_{max} - \theta^{i+1}_{max})}{\theta^{i}_{max}}\right| < 2 \times 10^{-4} \tag{25}$$

The appropriate mesh size is found when the Eq. (25) is satisfied. The refined mesh "$i + 1$" has approximately four times more finite elements in comparison with the previous coarse mesh "i". The refinement process is repeated up to the grid independence criterion was achieved. The grid independent mesh is reached for 20,486 triangular elements, which is adequate for the present diffusive dominant problem. Fig. 2 illustrates the grid independence study performed for one specific configuration where it is varied the θ_{max} as a function of the number of elements. It is shown the coarse mesh with 1265 elements and the independent grid with 20,486 elements. Meshes with similar configurations are employed in the remaining investigation. To verify the computational model, the present configuration (double Y) is degenerated in a cavity with a T configuration, allowing the comparison of the results for θ_{max} with those previously predicted in the literature [26,28,39], as illustrated in Table 1.

To validate and verify the computational method, one additional case is solved and compared with the experimental and numerical study of Cabezas et al. [53]. The case considers a steady state condition and consists of a solid cylinder with a diameter $d = 33$ mm, a length $l = 168$ mm, and a thermal conductivity in the range $k = 40$–45 W/(m·K) subjected to a heat flux in its inferior surface, as illustrated in Fig. 3(a). Part of the peripheral surface of the cylinder (-50 mm $\leq z < 0$ mm) is thermally insulated to direct the heat flux in the azimuth z-direction. The remaining peripheral surface (0 mm $\leq z \leq 118$ mm) is subjected to an enclosure environment with air as working fluid with T_{amb} measured experimentally. In the experiment, the temperatures T_0 ($z_0 = 0$ mm), T_3 ($z_3 = 118$ mm), and T_{amb} are used as input data for the solution of the numerical method, while the temperatures T_1 and T_2, measured in positions $r_1 = 16.5$ mm, $z_1 = 75$ mm and $z_2 = 95$ mm, are the outcome used

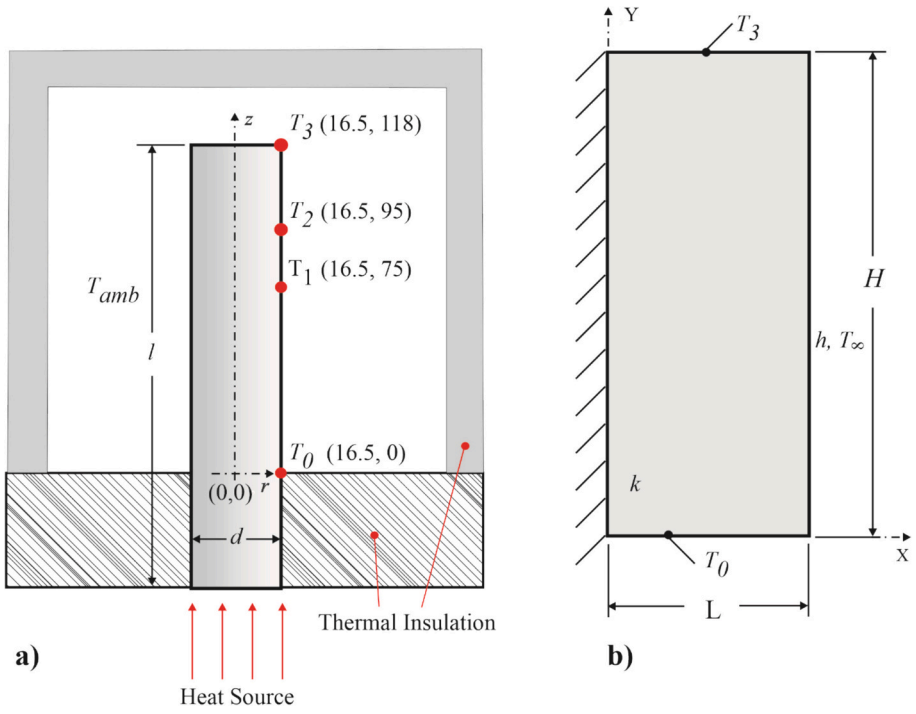

Fig. 3. Sketch of the problem used in validation of the computational method: a) experiment performed in Ref. [45] (dimensions in mm), b) computational domain used in the present work.

Table 2
Validation/Verification of the present model with temperature fields predicted experimentally and numerically by Cabezas et al. [53].

Case	T_1 (r_1 = 16.5 mm, z_1 = 75 mm) (°C)				T_2 (r_2 = 16.5 mm, z_2 = 95 mm) (°C)			
	Present	Ref. [53]			Present	Ref. [53]		
	FEM	Experiment	FD	FEM	FEM	Experiment	FD	FEM
1	34.45	33.9 ± 0.8	33.43	34.44	34.00	33.7 ± 0.8	34.00	33.98
2	36.16	35.5 ± 0.8	36.15	36.16	35.81	35.7 ± 0.8	35.80	35.79
3	50.44	49.6 ± 0.9	50.51	50.53	49.59	49.5 ± 0.9	49.57	49.55

to validate a numerical method. It is worth mentioning that the experiment is configured to prevent heat flux in the angular direction, and then a two-dimensional solution in a Cartesian coordinates system represents adequately the thermal field in this specific problem.

Fig. 3(b) represents the rectangular computational domain used here for the validation case. The problem has a height of $H = 118$ mm and a length of $L = 16.5$ mm. Moreover, a constant thermal conductivity $k = 42.5$ W/(m·K) is considered in all simulations. As performed in the numerical model used by Cabezas et al. [53], prescribed temperatures measured experimentally were adopted in the extremities of the cylinder: $z = 0$ mm (T_0) and $z = 118$ mm (T_3). An adiabatic boundary condition is considered at the left surface of the rectangle ($x = 0$ mm). A convection boundary condition with prescribed convection heat transfer coefficient (h) and enclosure temperature (T_{amb}) is considered in the right lateral surface. The coefficient h used in the validation simulation is as given by:

$$h = \frac{Nu_H k_{air}}{H} \tag{26}$$

where k_{air} is the thermal conductivity of the air (W/m·K), and Nu_H is the Nusselt number predicted for an ascending plume in an isothermal wall. The Nu_H is defined by the correlation of Churchill and Chu [46], which for an air flow with Prandtl number ($Pr = 0.72$) is given by:

$$Nu_H = \left(0.825 + 0.325 Ra_H^{1/6}\right)^2 \tag{27}$$

where Ra_H is the Rayleigh number given by:

$$Ra_H = \frac{g\beta\Delta T H^3}{\alpha\upsilon} \tag{28}$$

where g is the gravitational acceleration (m/s^2), β is the thermal expansion coefficient (K^{-1}), ΔT is the temperature difference ($\Delta T = T_0 - T_{amb}$), α is the thermal diffusivity of the air (m^2/s), and υ is the kinematic viscosity (m^2/s).

Table 2 presents a comparison among the temperatures T_1 and T_2 obtained with the present computational method and the experimental and numerical predictions of Cabezas et al. [53] based on the one-dimensional finite difference (FDM) and two-dimensional finite elements methods (FEM). Three different cases, with different temperatures for T_0, T_3 and T_{amb}, are evaluated: Case 1 – $T_0 = 36.1$ °C, $T_3 = 33.5$ °C, and $T_{amb} = 30.7$ °C; Case 2 – $T_0 = 37.5$ °C, $T_3 = 35.4$ °C, and $T_{amb} = 31.6$ °C; Case 3 – $T_0 = 54.1$ °C, $T_3 = 48.5$ °C, and $T_{amb} = 36.7$ °C.

Results of Table 2 indicated that the numerical results obtained with the present method presented a good agreement with the experimental and numerical results of Ref. [53]. The mean deviation in comparison with experimental measurements was around 1.1 %. Regarding the numerical predictions of Ref. [53], the deviations were even lower. Additionally, all predictions obtained with the present code conducted to deviations lower than the uncertainty of the experiment. Based on this comparison, it can be assumed that the present code is validated and verified, being adequate for the geometric investigation performed in the present work.

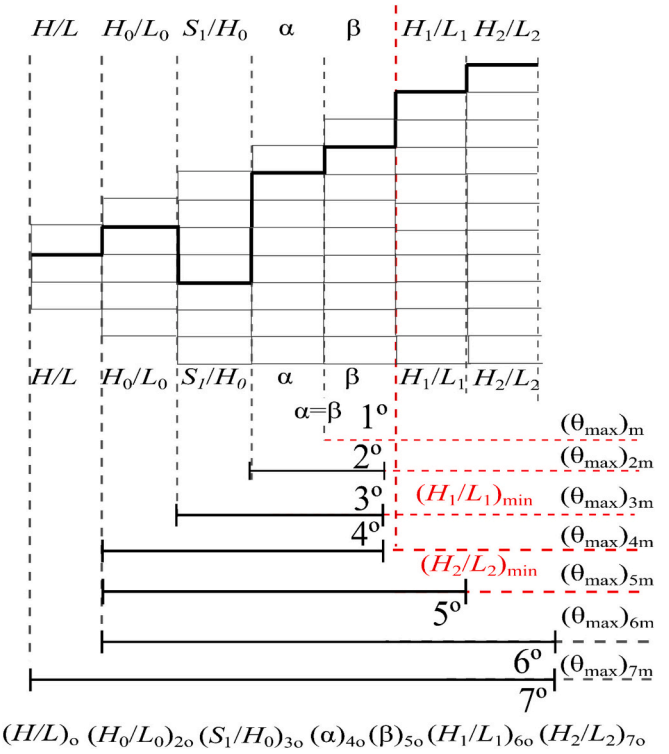

Fig. 4. Scheme for optimization of the cavity in form of double Y using the association among constructal design, exhaustive search, and differential evolution.

3. Optimization methodology

3.1. Constructal design of double Y-shaped cavity

The geometry optimization consists of applying the CD method for defining constraints, performance indicator, DOFs, and search space. The DE algorithm is applied to sweep the possibilities of finding the optimal configurations. In several cavity studies, the ES was used to optimize the geometric configurations, see Refs. [28–31, 37–43]. However, with the increase in DOFs number, their application has been restricted due to the increase in computational effort. Therefore, the ES method was associated with DE for optimizing the fourth DOF onward and reproducing the effect of the DOFs over the thermal performance and corresponding optimal configurations. It is worth mentioning that the validation of the present methodology for reproducing the DOFs effect over θ_{max} and corresponding optimal configurations for problems up to three DOFs was performed in Ref. [32].

The seven degrees of freedom (DOFs) that determine the geometry of a double Y-shaped cavity (H/L, H_0/L_0, S_1/H_0, α, β, H_1/L_1, and H_2/L_2) are varied in the optimization process seeking the optimal solution. The problem is subject to the area constraints φ_c, φ_1, and φ_2. The search space of DOFs is discrete and was generated dynamically according to the geometric limits. The DOFs have an interdependence between

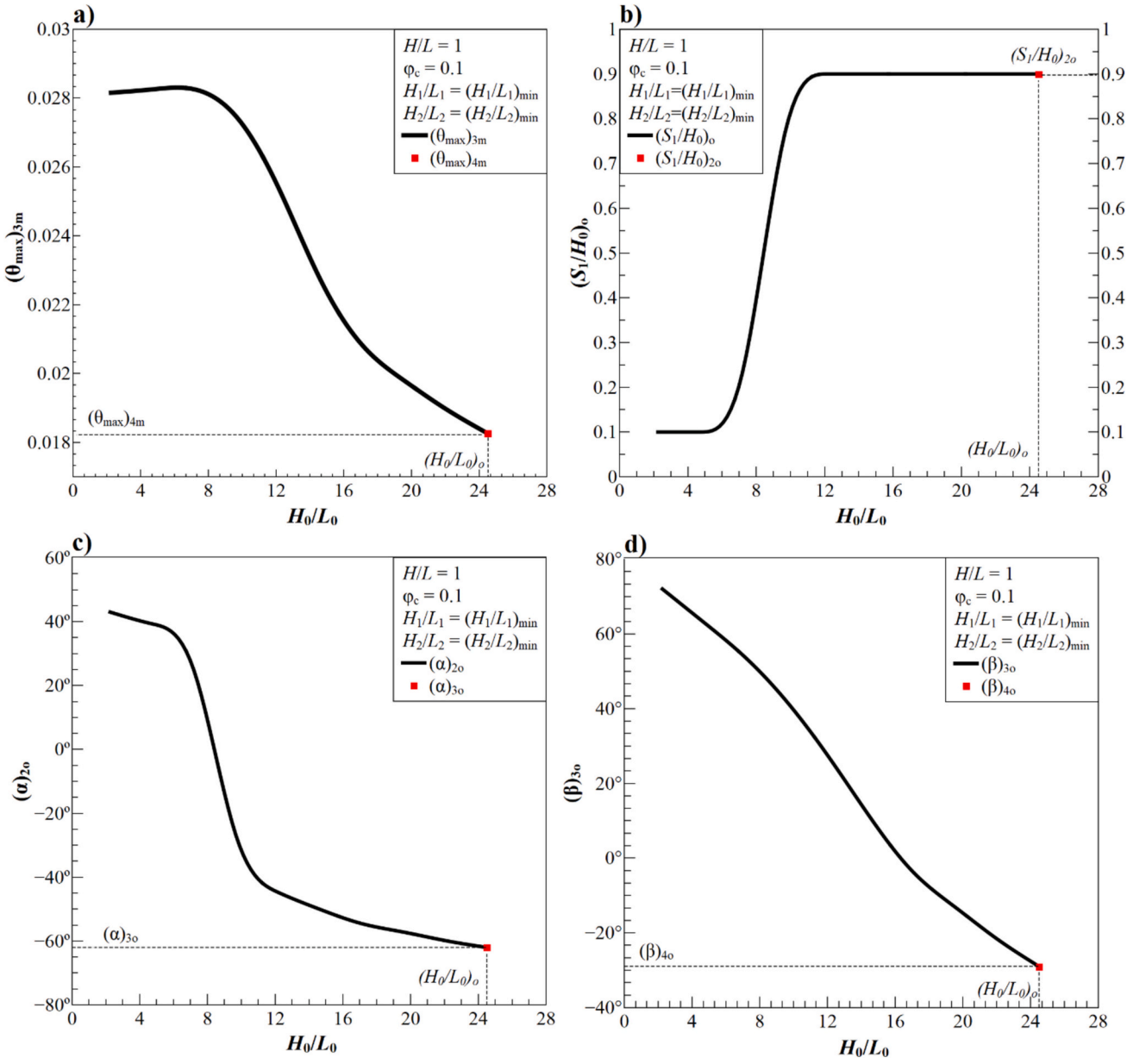

Fig. 5. Effect of H_0/L_0 reproduced by the DE1 over: a) $(\theta_{max})_{3m}$, b) $(S_1/H_0)_o$, c) $(\alpha)_{2o}$, d) $(\beta)_{3o}$.

themselves. Then, it is necessary to calculate the maximum and minimum values that each DOF can assume to generate the search space. The equations to determine the search space of the DOFs for each optimization level are presented later.

Fig. 4 shows the optimization levels in a diagram with the DOFs ordered according to their dependency hierarchy. The bolder pathway in the diagram of Fig. 4 represents the optimal geometry path among the geometric configuration possibilities indicated by light lines. Due to the investigation of many DOFs and the use of some strategies of investigation as the consideration of the minimal magnitudes for H_1/L_1 and H_2/L_2 in the study of the first four DOFs, the diagram in Fig. 4 replaces the tree flowchart commonly presented in the literatures [13,26]. In Fig. 4, the optimization from the 1st to 7th levels is represented by horizontal lines, indicating the optimized DOFs for each level. The study of Gonzales et al. [32] performed the optimization process up to the third level. This work considers the optimization from the fourth level onwards, i.e., the effect of H_0/L_0 over $(\theta_{max})_{4m}$ considering minimum magnitudes for (H_1/L_1) and (H_2/L_2), $(H_1/L_1)_{min}$ and $(H_2/L_2)_{min}$. The optimization in the fourth level, as shown in Fig. 4, includes the investigation of $(H_0/L_0)_o$, as well as the search for $(S_1/H_0)_{2o}$, $(\alpha)_{3o}$, and $(\beta)_{4o}$, in the achievement of the four times minimized maximum excess of temperature, represented by $(\theta_{max})_{4m}$. As can be seen in Fig. 4, for the fourth level of optimization studied here, the DOFs H_1/L_1 and H_2/L_2 were maintained at the minimal magnitudes according to the following equations:

$$(H_1/L_1)_{min} \cong \frac{\varphi_1}{\left(\frac{\frac{L_0}{2}-\frac{L_0}{2}-0.01}{cos|\alpha|}\right)^2} \tag{29}$$

$$(H_2/L_2)_{min} \cong \frac{\varphi_2}{\left(\frac{\frac{L_0}{2}-\frac{L_0}{2}-0.01}{cos|\beta|}\right)^2} \tag{30}$$

Once Eqs. (29)–(30) can achieve configurations with restricted space between the cavity and external surfaces of the solid, degenerating the domain, the algorithm considers that this kind of configuration is

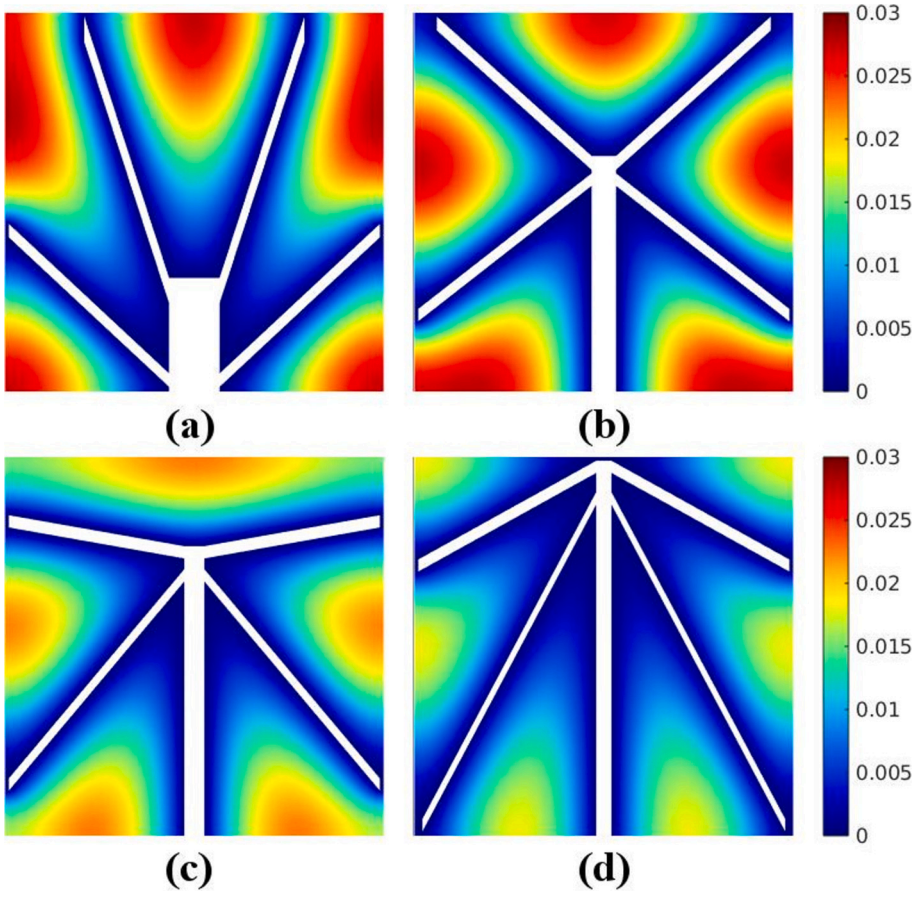

Fig. 6. Optimal geometries for the effect of H_0/L_0 over $(\theta_{max})_{3m}$: a) $H_0/L_0 = 2.25$, $(S_1/H_0)_o = 0.1$, $(\alpha)_{2o} = 43°$, $(\beta)_{3o} = 72°$, $(\theta_{max})_{3m} = 0.0281$; b) $H_0/L_0 = 9.66$, $(S_1/H_0)_o = 0.9$, $(\alpha)_{2o} = -38°$, $(\beta)_{3o} = 42°$, $(\theta_{max})_{3m} = 0.0276$; c) $H_0/L_0 = 14.61$, $(S_1/H_0)_o = 0.9$, $(\alpha)_{2o} = -50°$, $(\beta)_{3o} = 10°$, $(\theta_{max})_{3m} = 0.0225$; d) $(H_0/L_0)_o = 24.50$, $(S_1/H_0)_{2o} = 0.9$, $(\alpha)_{3o} = -62°$, $(\beta)_{4o} = -29°$, $(\theta_{max})_{4m} = 0.0182$.

invalid, generating an exception, and the magnitude of θ_{max} associated with this condition is equal to infinity. The calculus of $(H_1/L_1)_{min}$ and $(H_2/L_2)_{min}$ is important to generate a valid search space during optimization. The minimal values for the branches followed recommendations indicated in the results of [26,39], which seems a reasonable recommendation since most of the investigated isothermal cavities improved their performance when the cavity had a step intrusion into the solid domain [26,28,29,42–46]. These recommendations for H_1/L_1 and H_2/L_2 are not employed for the fifth optimization level onward. For the fifth and sixth levels of optimization, the ratios H_1/L_1 and H_2/L_2 are free to vary and optimized, reaching the $(\theta_{max})_{6m}$ and the corresponding optimal configurations. The results of the fifth and sixth levels of geometric optimization of the double Y-shaped cavity also verify if using minimal values for the branches is an adequate recommendation for the lowest optimization levels.

The complete optimization of the geometry includes the investigation of the ratio of H/L, concerned with the solid domain, maintaining the constraints (φ_c, φ_1, and φ_2) fixed. For this optimization level, the objective is to reproduce the effect of H/L over the $(\theta_{max})_{6m}$ and the corresponding optimal geometries. In the last investigation, it is reproduced the effect of H/L over $(\theta_{max})_{6m}$ and optimal geometries for different values of constraints φ_c, φ_1, and φ_2. Therefore, the effect of the constraints is investigated over the seven times minimized dimensionless maximum excess of temperature $(\theta_{max})_{7m}$.

3.2. Differential evolution algorithm approach for design optimization

The DE algorithm is associated with the CD to evaluate a double Y-shaped cavity in the present work. Although using the DE meta-heuristic reduces the computational effort, the ES method is also needed to reproduce the effect of the geometry variation over optimal geometries and performance indicator, as recommended in the previous investigation of Gonzales et al. [32]. So, this work performs a hybrid methodology between ES and DE optimization methods.

The DE algorithm to be associated with CD was developed in the recent work of Gonzales et al. [32]. It is performed by a classical proposed DE algorithm, also named *rand/1/bin* that defines its mutation operator. Other alternative strategies can be used with different mutation operators, for example, varying the number of vectors evolved [54–56]. Another mutation parameter used in this work is *best/2/bin*, also proposed by Storn and Price [57]. A third mutation parameter applied in the optimization process is a variation of *best/2/bin* called *best/1/bin*. All mutation operators (*rand/1/bin*, *best/2/bin*, and *best/1/bin*) are, respectively, represented by the following equations:

$$v_{i,G+1} = x_{r_1,G} + F \times \left(x_{r_2,G} - x_{r_3,G}\right) \tag{31}$$

$$v_{i,G+1} = x_{best,G} + F \times \left(x_{r_1,G} + x_{r_2,G} - x_{r_3,G} - x_{r_4,G}\right) \tag{32}$$

$$v_{i,G+1} = x_{best,G} + \mathrm{F} \times \left(x_{r_1,G} - x_{r_2,G}\right) \tag{33}$$

Gonzales et al. [32] extensively investigated the parameters of the DE algorithm when employed in the geometrical optimization of the cavity in the form of double Y. Statistical methods validated the results of Gonzales et al. [32] and the conclusions pointed that the best performance of the DE algorithm was achieved when it used the following parameters for amplification factor and crossover rate: $F = 1$, $CR = 0.9$. Therefore, the present work also uses these parameters to configure different versions of the DE algorithm, named DE1, DE2, and DE3, which

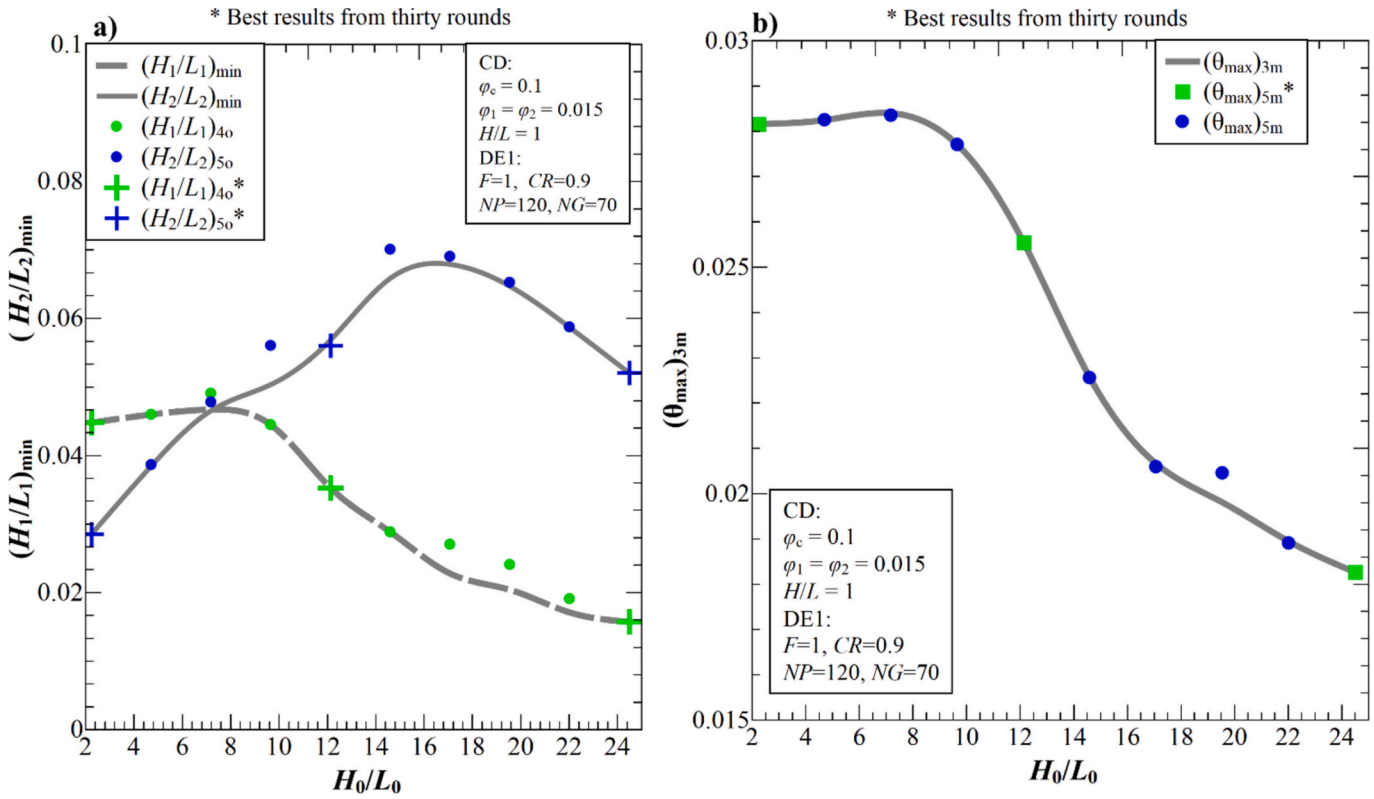

Fig. 7. Comparison of the effect of H_0/L_0 over the: a) $(H_1/L_1)_{4o}$, $(H_2/L_2)_{5o}$ and $(H_1/L_1)_{min}$, $(H_2/L_2)_{min}$; b) $(\theta_{max})_{3m}$ and $(\theta_{max})_{5m}$.

use the Eqs. (31)–(33), respectively.

4. Results and discussion

4.1. Optimization of four DOFs

In this section, the optimization seeks the optimal geometries of the three degrees of freedom for each value of the ratio H_0/L_0 in the search space composed by discrete linear values in the interval between $2.25 \leq H_0/L_0 \leq 24.5$ generated by the *linspace* function of MATLAB® software [52]. The limits in the search space of H_0/L_0 are defined by the height of the solid domain and the cavity fraction area (φ_c). The aim is to reproduce the effect of H_0/L_0 over $(\theta_{max})_{3m}$ and corresponding optimal configurations ($(S_1/H_0)_o$, $(\alpha)_{2o}$, and $(\beta)_{3o}$). For the fourth level optimization, the domain aspect ratio was kept at $H/L = 1$, and the area constraints were defined with $\varphi_c = 0.1$ and $\varphi_1 = \varphi_2 = 0.015$. For the investigation of this section, the DE1 algorithm is used, following the recommendation of Ref. [32], with $NP = 45$ and $NG = 75$.

Fig. 5 shows the effect of H_0/L_0 over the $(\theta_{max})_{3m}$ and the corresponding optimal configurations: $(S_1/H_0)_o$, $(\alpha)_{2o}$, and $(\beta)_{3o}$, given respectively by Fig. 5 (a) – (d). It can be noticed for $(\theta_{max})_{3m}$ a region of stabilization in the range $2.0 \leq H_0/L_0 \leq 8.0$ followed by a step decrease for $H_0/L_0 > 8.0$ up to the superior limit of $(H_0/L_0)_o = 24.5$, where the optimal configuration is reached. As noticed for S_1/H_0, the highest magnitude of H_0/L_0 led to the best performance, i.e., when the trunk has the highest intrusion into the solid domain. Fig. 5 (b) shows the effect of H_0/L_0 over the $(S_1/H_0)_o$, being possible to observe that for $H_0/L_0 \leq 5$ the optimal value of $(S_1/H_0)_o = 0.1$, i.e., when the cavity has a smaller height, the optimal position of the inferior branches is in the bottom of the solid. When the cavity height grows, $H_0/L_0 > 8$, the optimal geometry of $(S_1/H_0)_o$ increases up to the highest possible magnitude, $(S_1/H_0)_{2o}$. This effect is only possible due to the possibility of the angle α to assume negative values. For $H_0/L_0 > 8$, the optimal angle of $(\alpha)_{2o}$ changed from positive to negative magnitudes, Fig. 5(c), distributing the inferior branches of the cavity from the upper central region of the solid domain towards the inferior corners of the domain and distributing the temperature fields in the central and inferior regions. Fig. 5(c) also illustrates that when H_0/L_0 is small, the inferior branches have a step positive angle, $(\alpha)_{2o} > 40°$, avoiding the increase of temperature in the central superior region of the solid domain. In the region $7 < H_0/L_0 < 9$, an abrupt fall in the magnitude of $(\alpha)_{2o}$ from positive to negative magnitudes is noticed. For the highest magnitudes of H_0/L_0, the rate of decrease of $(\alpha)_{2o}$ turns to stabilize. Fig. 5(d) shows the effect of H_0/L_0 over $(\beta)_{3o}$, as well as the four times optimized angle of $(\beta)_{4o}$. It is possible to see that the transition from positive to negative angles is not as steep as the angle $(\alpha)_{2o}$. The negative magnitudes of $(\beta)_{3o}$ are observed only for $H_0/L_0 > 16$. This behavior is related to the position of the superior branches placed in the upper region of the solid domain. Consequently, these branches are not used for cooling the inferior region of the solid domain. Despite that, the four times optimized angles $(\beta)_{4o}$ are obtained for negative values, being the trunk responsible for cooling the superior region of the solid domain.

To illustrate the effect of H_0/L_0 over the thermal fields and cavity design, Fig. 6 shows the temperature fields in the domain for four different magnitudes of H_0/L_0: $H_0/L_0 = 2.25$, Fig. 6(a), $H_0/L_0 = 9.66$, Fig. 6(b), $H_0/L_0 = 14.61$, Fig. 6(c), and $(H_0/L_0)_o = 24.50$, Fig. 6(d). The configurations shown in Figs. 6(a) – (c) can represent a sort of geometric evolution from previous configurations investigated in the literature as T, X, and Y [28,29,39] with a new structure of design inserted in the domain, i.e., the inferior branches. Fig. 6(d) shows a configuration like the tree-shaped roots of leaves, with different angles α and β, thicknesses, and lengths of the branches. It can also be observed that the highest difference in the thermal performance is noticed when the number of hot regions changed from five to six, reinforcing that the evolution of the design is related to the best distribution of the imperfections, i.e., following the constructal law.

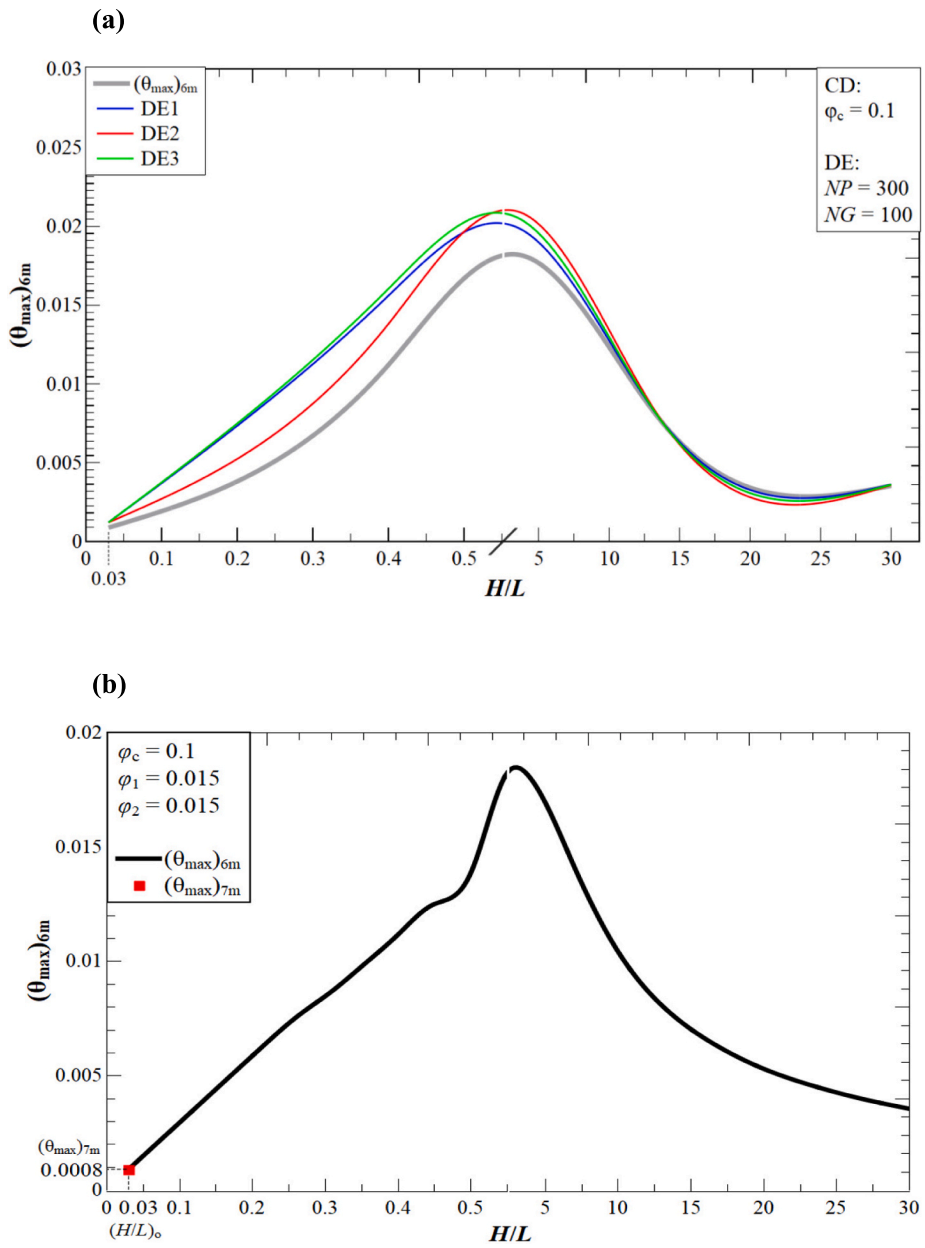

Fig. 8. Effect of H/L over $(\theta_{max})_{6m}$: a) comparison among different DE versions, b) minimal values achieved for $(\theta_{max})_{6m}$.

4.2. Optimization of five and six DOFs

The geometric evaluation of five and six degrees of freedom of the double Y-shaped cavity comprises the optimization of the H_1/L_1 and H_2/L_2 ratios for different values of H_0/L_0. The objective is to reproduce the effect of H_0/L_0 over the performance indicator of $(\theta_{max})_{5m}$ and over the optimal geometries of $(H_1/L_1)_{4o}$ and $(H_2/L_2)_{5o}$. In this section, it is also investigated the optimal configurations $(H_0/L_0)_o$, $(S_1/H_0)_{2o}$, $(\alpha)_{3o}$, $(\beta)_{4o}$, $(H_1/L_1)_{5o}$, $(H_2/L_2)_{6o}$ and performance indicator $(\theta_{max})_{6m}$. This section also aims to verify if the recommendation of the minimal values used for H_1/L_1 and H_2/L_2 in the previous optimization steps is adequate. Therefore, the problem is the same as analyzed in section 4.3, for the same search space of H_0/L_0 and using the same values for H/L and constraints (φ_c, φ_1, and φ_2).

The optimization process is performed by the DE algorithm versions DE1, DE2, and DE3. It uses the same parameters of the previous section, except for the parameters *NP* and *NG*, which are tested with several combinations, but all limited to a total number of 5000 and 6000 simulations for the sole optimization of H_2/L_2 and optimization of both DOFs (H_1/L_1 and H_2/L_2). The first experiment is the optimization of H_2/L_2 and keeping the H_1/L_1 with the minimal values, according to section 3.1. The second experiment optimizes the sixth level, where both ratios (H_1/L_1 and H_2/L_2) are optimized. The choice for the parameters *NP* and *NG* is made based on the execution of thirty runs for three ratios of H_0/L_0.

Fig. 7 illustrates the effects of H_0/L_0 over $(\theta_{max})_{5m}$, Fig. 7(a), and the DOFs $(H_1/L_1)_{4o}$, and $(H_2/L_2)_{5o}$, Fig. 7(b). These effects are reproduced by the DE1 version of the DE algorithm, with $NP = 120$ and $NG = 70$. The cross-shaped symbols in Fig. 7 represent the optimal values reached during the 30 runs of the algorithm for specific values of H_0/L_0. The other results represented by points are the optimal values achieved for just one round obtained with the algorithm DE1. The gray curves in both Figs. 7(a) and (b) represent the effect of H_0/L_0 over the $(\theta_{max})_{3m}$ and the magnitudes of $(H_1/L_1)_{min}$, $(H_2/L_2)_{min}$ for each H_0/L_0, obtained in the previous optimization level for four degrees of freedom, when the minimal values of H_1/L_1 and H_2/L_2 are established by Eqs. (1) and (2),

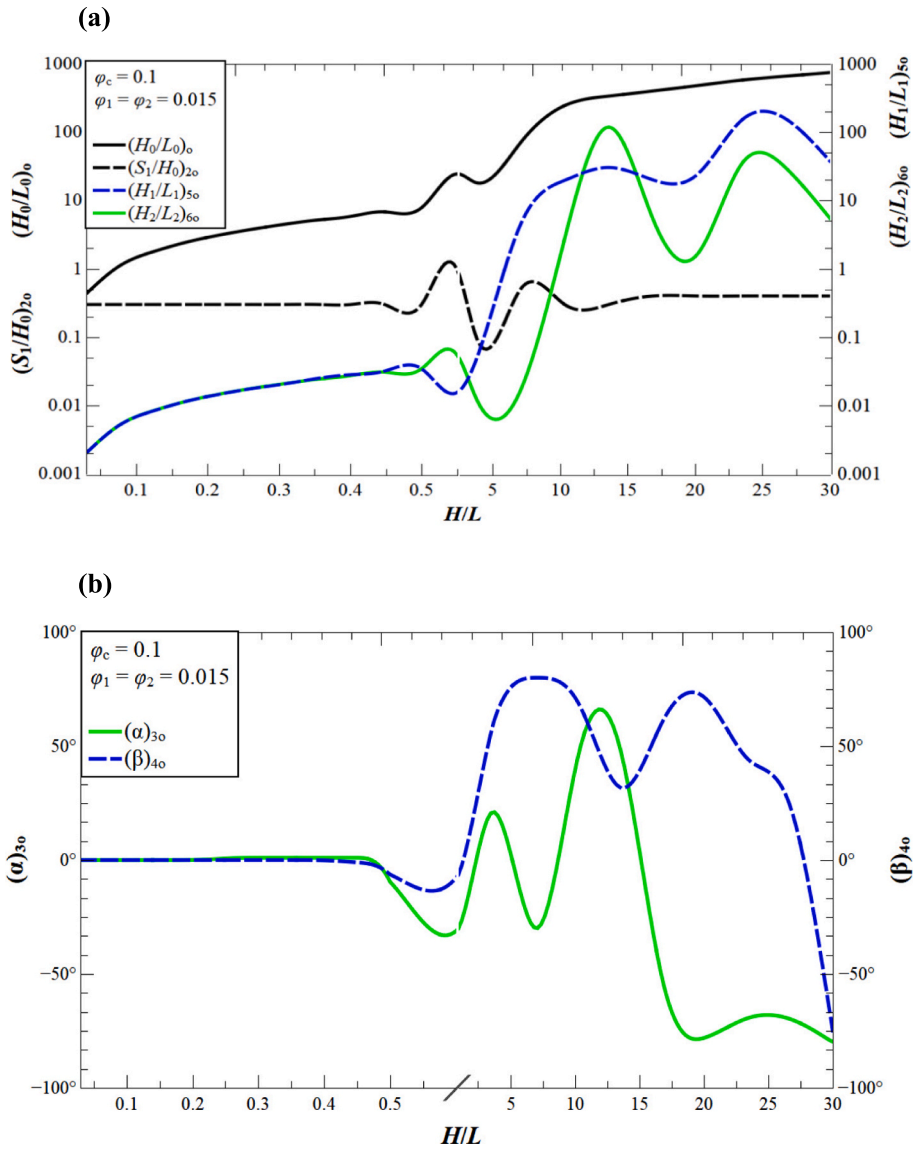

Fig. 9. Effect of H/L over six times optimized geometries: a) $(\alpha)_{3o}$ and $(\beta)_{4o}$; b) $(H_0/L_0)_o$, $(S_1/H_0)_{2o}$, $(H_1/L_1)_{5o}$,and $(H_2/L_2)_{6o}$.

see Fig. 5. Fig. 7 indicates that the values reached with the DE1 algorithm for the effect of H_0/L_0 over $(H_1/L_1)_{4o}$ and $(H_2/L_2)_{5o}$ are very similar to that considered for $(H_1/L_1)_{min}$ and $(H_2/L_2)_{min}$, Fig. 7(b). The same behavior can be observed in Fig. 7(a) for the effect of H_0/L_0 over $(\theta_{max})_{5m}$ and $(\theta_{max})_{3m}$, except for $H_0/L_0 = 19.5$, when the algorithm of DE1 reaches a local minimum, but nearest to the optimal configuration that conducted to $(\theta_{max})_{3m}$. Furthermore, some values achieved by the DE1 version for $(H_1/L_1)_{4o}$ and $(H_2/L_2)_{5o}$ did not converge exactly to the same curves of $(H_1/L_1)_{min}$ and $(H_2/L_2)_{min}$, but these errors do not affected significantly the values of $(\theta_{max})_{5m}$.

Finally, the optimal geometry for the cavity six times optimized is the same obtained in Fig. 6(d), represented by the green box in Fig. 7(b) for the highest magnitude of H_0/L_0. The optimal configuration geometry achieved has the following configurations: $(H_0/L_0)_o = 24.5$, $(S_1/H_0)_{2o} = 0.9$, $(\alpha)_{3o} = -62°$, $(\beta)_{4o} = -29°$, $(H_1/L_1)_{5o} = 0.0156$, and $(H_2/L_2)_{6o} = 0.0519$, which lead to $(\theta_{max})_{6m} = 0.0182$. Therefore, the algorithm DE1 converged to the same values predicted with minimal ratios of $(H_1/L_1)_{min}$ and $(H_2/L_2)_{min}$, reinforcing the suitability of the previous consideration, which can be used for similar cases and conditions in the future. The results also reinforced that, for cavities with a high capacity to remove heat from the solid (isothermal or high magnitudes of coefficient h), the highest intrusion of the cavity into the solid domain is beneficial for thermal performance.

4.3. Optimization of seven DOFs

The seventh optimization level consists of optimizing all degrees of freedom, including the ratio of the solid, H/L. The process seeks the optimal geometric configuration of the six DOFs $(H_0/L_0)_o$, $(S_1/H_0)_{2o}$, $(\alpha)_{3o}$, $(\beta)_{4o}$, $(H_1/L_1)_{5o}$, and $(H_2/L_2)_{6o}$ for each value of the discrete search space of H/L. Moreover, it aims to reproduce the effect of H/L over $(\theta_{max})_{6m}$ and the corresponding optimal DOFs. Before performing the complete optimization process for all values in the search space of H/L, the algorithm versions of DE (DE1, DE2, and DE3) were executed for some ratios of H/L, and the parameters of NP and NG were adjusted to the problem. Each algorithm uses the same parameters of population size and total generation number of $NP = 300$ and $NG = 100$. Another stop criterion is imposed on the algorithm to reduce the number of simulations. More precisely, it is considered that when the standard deviation of $(\theta_{max})_{6m}$ is lower than 1×10^{-3}, the algorithm is stopped, even if the number of generations is lower than the NG parameter.

Fig. 8 shows the effect of H/L over $(\theta_{max})_{6m}$. More precisely, Fig. 8(a) shows the experiment results that execute thirty runs for each version of the DE algorithm and five values of H/L. Fig. 8(a) shows the average

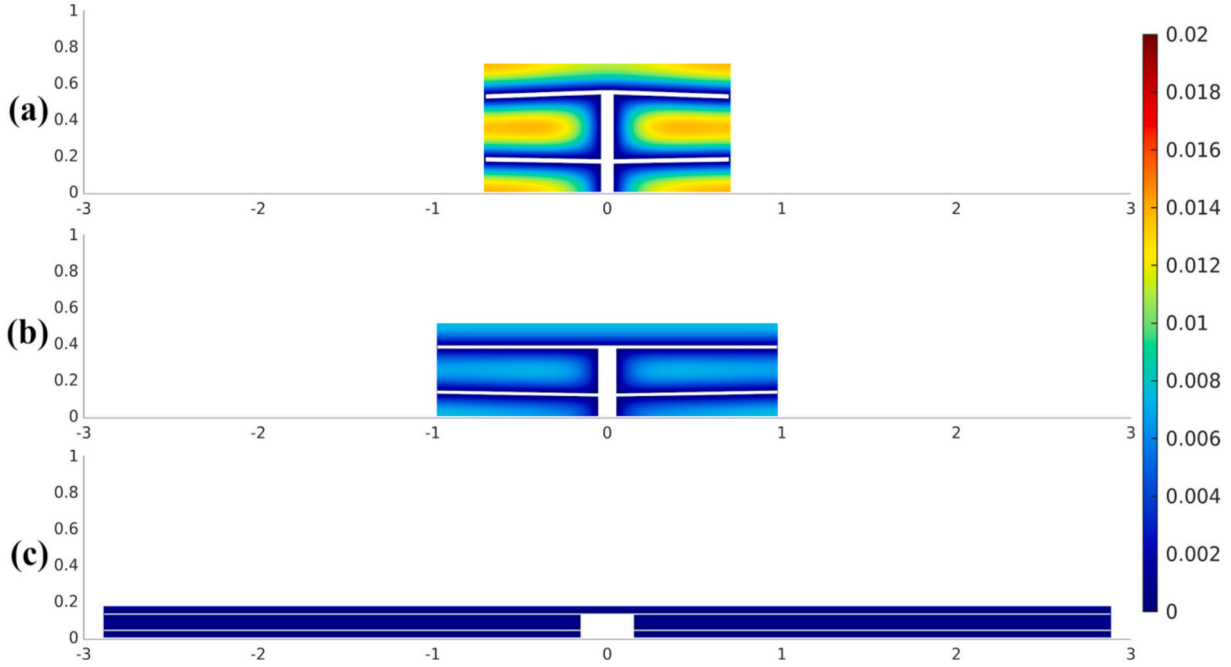

Fig. 10. Optimal geometries for different ratios of $H/L \leq 0.5$: a) $H/L = 0.5$, $(H_0/L_0)_o = 7.84$, $(S_1/H_0)_{2o} = 0.3$, $(\alpha)_{3o} = 1°$, $(\beta)_{4o} = -2°$, $(H_1/L_1)_{5o} = 0.0343$, $(H_2/L_2)_{6o} = 0.0343$, $(\theta_{max})_{6m} = 0.0138$; b) $H/L = 0.26$, $(H_0/L_0)_o = 3.78$, $(S_1/H_0)_{2o} = 0.3$, $(\alpha)_{3o} = 1°$, $(\beta)_{4o} = 0°$, $(H_1/L_1)_{5o} = 0.0176$, $(H_2/L_2)_{6o} = 0.0177$, $(\theta_{max})_{6m} = 0.0075$; c) $(H/L)_o = 0.03$, $(H_0/L_0)_{2o} = 0.43$, $(S_1/H_0)_{3o} = 0.3$, $(\alpha)_{4o} = 0°$, $(\beta)_{5o} = 0°$, $(H_1/L_1)_{6o} = 0.002$, $(H_2/L_2)_{7o} = 0.002$, $(\theta_{max})_{7m} = 0.0008$.

values of $(\theta_{max})_{6m}$, represented by curves in different colors, reached for each DE algorithm and H/L analyzed. The gray curve represents the effect of H/L over the thermal performance using the minimal magnitudes of $(\theta_{max})_{6m}$ predicted among all the algorithms. Fig. 8(b) shows this curve in a clearer form. Fig. 8 indicates that the algorithms have more difficulty converging to the minimal values of $(\theta_{max})_{6m}$ for $H/L < 5$, especially for $H/L = 0.4$, where a large dispersion is obtained. On the contrary, for $H/L > 5$, all algorithms converged to the minimal values or close to it in all thirty runs. In general, results indicated that the algorithm performance varies according to the search space, showing the importance of adapting the algorithm parameters to the problem to be studied. Even when executing tests to adapt the parameters, the computational effort is significantly reduced compared to the sole application of ES for optimization. According to the effect shown in Fig. 8(b), it can be seen that the extreme ratios in the search space of H/L conduct the best thermal performances of the problem, being the $(\theta_{max})_{7m} = 8 \times 10^{-4}$ achieved for $(H/L)_o = 0.03$. On the other extreme, for $H/L = 30$, the magnitude is $(\theta_{max})_{6m} = 3.5 \times 10^{-3}$. The worst performance is $(\theta_{max})_{6m} = 1.82 \times 10^{-2}$ for $H/L = 1$. The optimal performance for $H/L = 0.03$ is related to the increase in the length of the cavity branches towards the lateral limits of the computational domain. Furthermore, the angles of the cavity branches $(\alpha)_{3o}$ and $(\beta)_{4o}$ are kept near 0° and assume a geometry like the cavity configured as double T [26]. However, for the other extreme in the search space, $H/L = 30$, the optimal cavity has a maximum height, and the bifurcated branches are degenerated, conducting an I-shaped configuration [28]. This behavior is expected since the lowest or highest ratios of H/L guide one preferential cavity construction, making it difficult to distribute the cavity along the solid with $H/L \sim 1.0$. This also leads to difficulties for optimization since more degrees of freedom have sensibility over the thermal performance. Fig. 9 shows the effect of H/L over the optimal geometries of $(H_0/L_0)_o$, $(S_1/H_0)_{2o}$, $(\alpha)_{3o}$, $(\beta)_{4o}$, $(H_1/L_1)_{5o}$, and $(H_2/L_2)_{6o}$, for $\varphi_c = 0.1$, $\varphi_1 = \varphi_2 = 0.015$. From the results of Fig. 9(a), it is possible to observe that the solid ratio H/L greatly influences the optimal geometry of the $(H_0/L_0)_o$. This DOF tends to grow proportionally to the rise of H/L, except for $H/L = 1$ where $(H_0/L_0)_o$ locally decreased. This effect shows that the cavity trunk height tries to follow the increase of the solid height to distribute the thermal field along the domain. A similar effect can be noticed for the cavity branches $(H_1/L_1)_{5o}$ and $(H_2/L_2)_{6o}$ for $H/L < 1$, where the cavity branches seek to stretch up to the lateral limits of the computational domain. The ratios $(H_1/L_1)_{5o}$ and $(H_2/L_2)_{6o}$ have the same magnitude up to $H/L = 0.5$. After this point, the values of both ratios diverge and have an oscillating behavior but show a mean growth tendency. Concerning the ratio $(S_1/H_0)_{2o}$, Fig. 9(a), the behavior is almost constant with the ratio H/L with values near to $(S_1/H_0)_{2o} = 0.3$. However, in the range $0.5 \leq H/L \leq 10$, an oscillation in the magnitudes of $(S_1/H_0)_{2o}$ can be noticed, The effect of H/L over $(\alpha)_{3o}$ and $(\beta)_{4o}$, Fig. 9 (b), presented optimal values for $H/L \leq 0{,}5$ near $(\alpha)_{3o} = (\beta)_{4o} = 0°$, which means that the optimal geometry of the cavity assumes a configuration of double T [26]. However, for $H/L > 0.5$, the angles of the cavity branches have more influence over the thermal performance of the system, mainly for $H/L = 1$. For $H/L > 5$, the angles $(\alpha)_{3o}$ and $(\beta)_{4o}$ presented a strong variation and did not influence the thermal resistance in comparison with other ratios, as $(H_0/L_0)_o$, $(S_1/H_0)_{2o}$, $(H_1/L_1)_{5o}$, and $(H_2/L_2)_{6o}$. For the highest values of H/L, the cavity assumed an I-shaped geometry [24], and the angles did not show sensibility over $(\theta_{max})_{6m}$.

Fig. 10 shows the optimal geometries achieved for some ratios of $H/L \leq 0.5$, $H/L = 0.5$, Fig. 10(a), $H/L = 0.26$, Fig. 8(b), $H/L = 0.03$, Fig. 8(c). All configurations for this range of H/L are like the optimal configurations reached for a double T configuration [26], which can be attested for the optimal angles $(\alpha)_{3o}$ and $(\beta)_{4o}$ obtained near 0°. The trunk is more robust for the lowest magnitudes of H/L, and the bifurcated branches are thin and slender, having a higher intrusion into the solid domain. For ratios of $H/L > 1$, some optimal geometries are represented in Fig. 11, as follows: $H/L = 3.77$, Fig. 11(a), $H/L = 10.33$, Fig. 11(b), and $H/L = 30$, Fig. 11(c). The first optimal geometry shown in Fig. 11(a) reaches a thermal performance like the cavity geometry achieved for $H/L = 1$ and assumes a tree-shaped pattern, widely seen in natural configurations as a leaf. The treelike pattern is not the most efficient for slender and tall solids, as the cavity degenerated into an I-shaped configuration. Figs. 10 and 11 also demonstrate that for the lowest and highest ratios of H/L, the point-to-volume flow is degenerated point-to-point by the solid constraint, affecting the design of the flow system. Moreover, in the present investigation, the treelike-shaped configuration tends to be

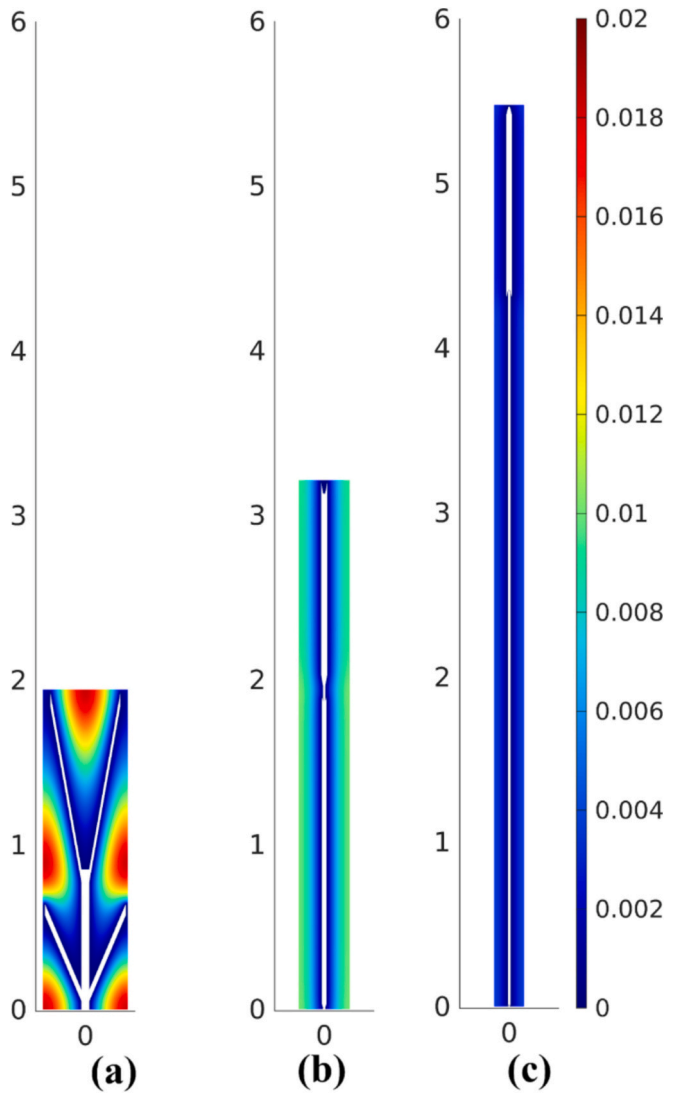

Fig. 11. Optimal geometries for different ratios of $H/L > 0.5$: a) $H/L = 3.77$, $(H_0/L_0)_o = 18.13$, $(S_1/H_0)_{2o} = 0.1$, $(\alpha)_{3o} = 67°$, $(\beta)_{4o} = 80°$, $(H_1/L_1)_{5o} = 0.0466$, $(H_2/L_2)_{6o} = 0.0124$, $(\theta_{max})_{6m} = 0.0181$; b) $H/L = 10.33$, $(H_0/L_0)_o = 254.27$, $(S_1/H_0)_{2o} = 0.3$, $(\alpha)_{3o} = 73°$, $(\beta)_{4o} = -80°$, $(H_1/L_1)_{5o} = 20.432$, $(H_2/L_2)_{6o} = 2.229$, $(\theta_{max})_{6m} = 0.0101$; c) $H/L = 30$, $(H_0/L_0)_o = 747.26$, $(S_1/H_0)_{2o} = 0.4$, $(\alpha)_{3o} = -80°$, $(\beta)_{4o} = -75°$, $(H_1/L_1)_{5o} = 37.75$, $(H_2/L_2)_{6o} = 5.48$, $(\theta_{max})_{6m} = 0.0035$.

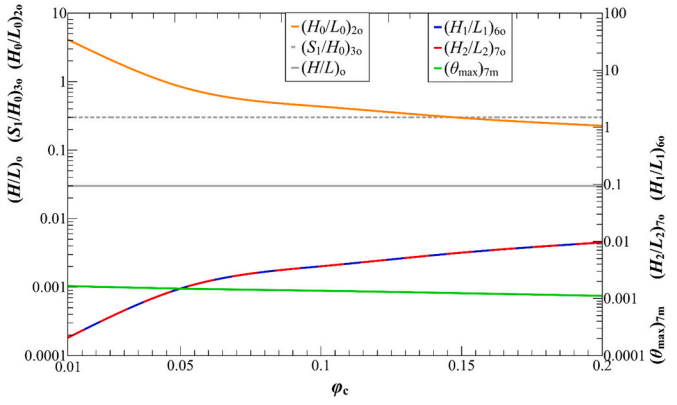

Fig. 12. Effect of φ_c over $(\theta_{max})_{7m}$ and the optimal configurations.

optimal for solids in the $1.0 \leq H/L \leq 3.77$ range.

4.4. Optimization for different cavity constraints

The evaluation of the constraints φ_c, φ_1, and φ_2 consisted of the complete optimization process for all DOFs varying the applied value for the cavity fraction area, $\varphi_c = [0.01, 0.05, 0.15, 0.2]$. The DE algorithm versions, DE1 and DE2, perform the complete optimization for different defined constraint values. The same optimization methodology presented in section 4.3 for complete optimization for $\varphi_c = 0.1$ was repeated for the different investigated constraints in this section. The DE2 algorithm version is chosen for the search space of $H/L < 1$, while DE1 is used for $H/L \geq 1$. Thirty runs were executed, and the minimum value reached is considered. The parameters of population numbers and total generations used were $NP = 100$ and $NG = 300$.

Fig. 12 shows the effect of φ_c over $(\theta_{max})_{7m}$, as well as the seven times optimized geometry, composed by $(H/L)_o$, $(H_0/L_0)_{2o}$, $(S_1/H_0)_{3o}$, $(H_1/L_1)_{6o}$ and $(H_2/L_2)_{7o}$. The optimal angles of the branches, $(\alpha)_{4o}$ and $(\beta)_{5o}$, were equal to 0° for all constraints evaluated and, for brevity, are not shown in Fig. 12. The degrees of freedom $(H/L)_o$ and $(S_1/H_0)_{3o}$ are also insensible to the variations of constraints, assuming the magnitudes $(H/L)_o = 0.03$ and $(S_1/H_0)_{3o} = 0.3$. The same behavior noticed for $\varphi_c = 0.1$, Fig. 8, concerned with the optimal configurations when $H/L << 1$, is also achieved for the other magnitudes of φ_c, i.e., the double-Y-cavity degenerated in a double T configuration. The effect of φ_c over $(H_0/L_0)_{2o}$, $(H_1/L_1)_{6o}$, and $(H_2/L_2)_{7o}$ in Fig. 12 represents the growth of the thickness of the stem and branches of the double T-shaped cavity.

The optimal geometries achieved for each φ_c evaluated are shown in Fig. 13. Fig. 13(a) shows the optimal geometry achieved for $\varphi_c = 0.01$, and the optimal geometry for the last constraint simulated, $\varphi_c = 0.2$, are shown in Fig. 13(e). Figs. 13(b) - 13(d) show the optimal configurations for intermediate magnitudes of $\varphi_c = 0.05$, $\varphi_c = 0.1$ and $\varphi_c = 0.15$, respectively. The optimal DOFs $(H/L)_o$, $(S_1/H_0)_{3o}$, $(\alpha)_{3o}$, and $(\beta)_{4o}$ are the same regardless of the magnitude of φ_c, assuming a double T configuration. Due to the area distribution between the cavity branches, the trunk of the cavity has 40 % of the cavity area and the branches 60 % for all configurations investigated until this point. Once the area of the trunk is constant, the decrease in the H/L ratio necessarily leads to an increase in the trunk thickness. To investigate different percentages of distribution between the trunk and branches of the cavities, considering $\varphi_1 = \varphi_2$, the same investigation performed in Figs. 12 and 13 is repeated for other percentages of the area of the branches, $\varphi_{1+2}/\varphi_c(\%) = 100\bullet(\varphi_1 + \varphi_2/\varphi_c)$, of 80 %, 90 %, and 95 %. Fig. 14 shows the new distribution of the shape for the different percentages of the area of the branches related to the cavity area: $\varphi_{1+2}/\varphi_c(\%) = 60$ %, Fig. 14(a), 80 %, Fig. 14(b), 90 %, Fig. 14(c), and 95 %, Fig. 14(d). In the present investigation, the distribution with the highest percentage for the branches leads to the best performance, i.e., $(\theta_{max})_{7m} = 6.7 \times 10^{-4}$, Fig. 14(d), which is almost 13 % superior to that reached for the configuration with 60 %, Fig. 14(a).

4.5. Comparison with other configurations studied in the literature

Finally, this section compares the performance obtained with the best shapes predicted with those obtained in the literature for different configurations investigated with constructal design. The purpose here is just to illustrate the differences in the global thermal performance for the several investigated configurations, showing how freedom can benefit the performance of isothermal cavities.

Table 3 compares the θ_{max} obtained for the double-Y-cavity configuration with others in the literature. For $H/L = 1.0$, commonly investigated in the literature and for the same conditions, significant differences of 81 %, 74 %, 70 %, 44 %, and 25 % are obtained when comparing the performance of double-Y-cavity with the H-, I-, T-, X-, and Y-shaped cavities [13,28,29,35–44]. For the square solid, the double-Y-cavity has a performance nearly 30 % superior to the double T

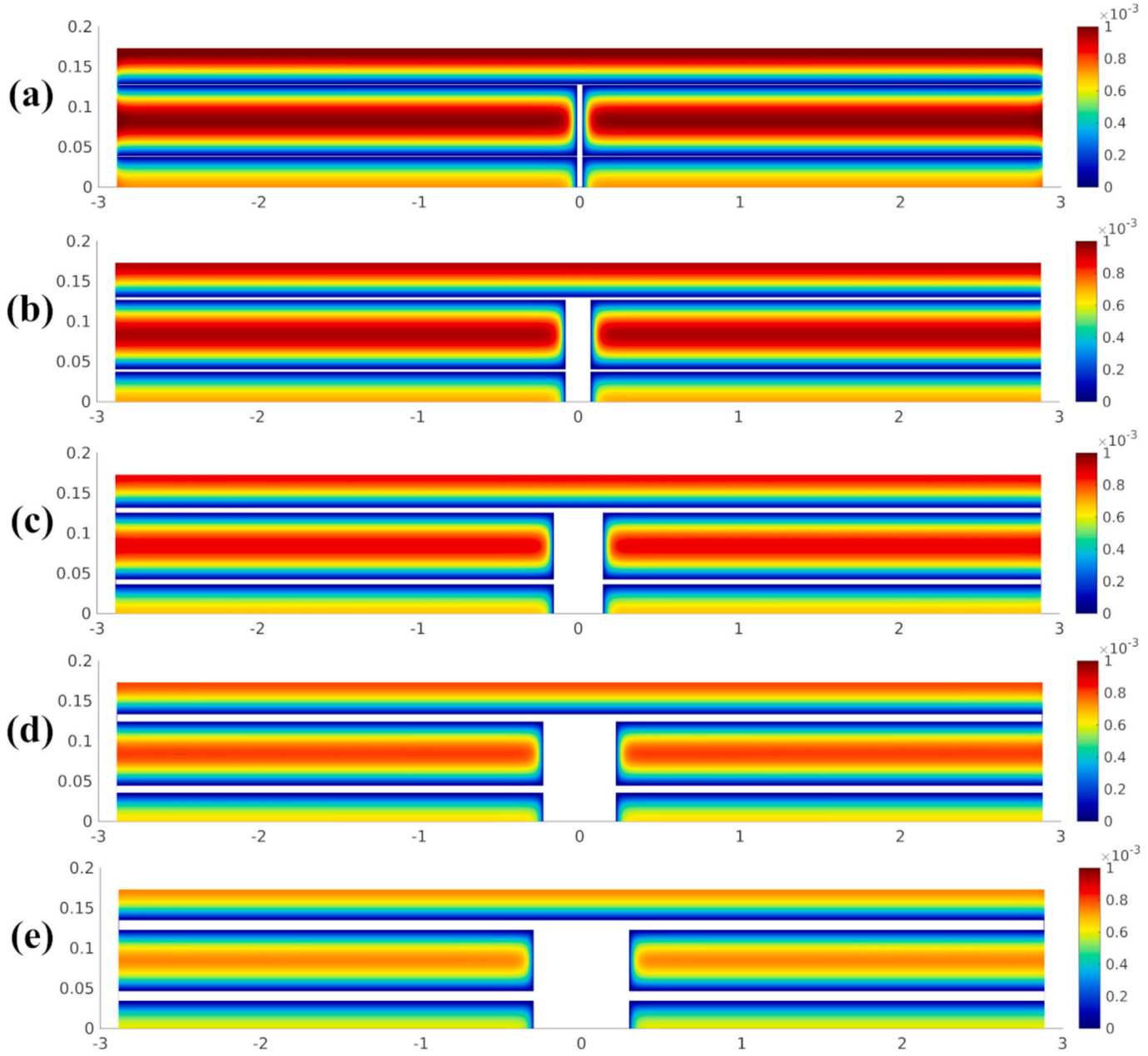

Fig. 13. Optimal geometries for different values of φ_c: a) $\varphi_c = 0.01$, $(H_0/L_0)_{2o} = 4.13$, $(H_2/L_2)_{6o} = (H_1/L_1)_{7o} = 0.00018$, $(\theta_{max})_{7m} = 1.01 \times 10^{-3}$; b) $\varphi_c = 0.05$, $(H_0/L_0)_{2o} = 0.84$, $(H_2/L_2)_{6o} = (H_1/L_1)_{7o} = 0.0009$, $(\theta_{max})_{7m} = 9.4 \times 10^{-4}$; c) $\varphi_c = 0.10$, $(H_0/L_0)_{2o} = 0.43$, $(H_2/L_2)_{6o} = (H_1/L_1)_{7o} = 0.002$, $(\theta_{max})_{7m} = 8.8 \times 10^{-4}$; d) $\varphi_c = 0.15$, $(H_0/L_0)_{2o} = 0.29$, $(H_2/L_2)_{6o} = (H_1/L_1)_{7o} = 0.003$, $(\theta_{max})_{7m} = 8.1 \times 10^{-4}$; e) $\varphi_c = 0.2$, $(H_0/L_0)_{2o} = 0.22$, $(H_2/L_2)_{6o} = (H_1/L_1)_{7o} = 0.004$, $(\theta_{max})_{7m} = 7.7 \times 10^{-4}$.

configuration. Compared with the Ψ-shaped cavity [30], the performance is nearly 1.0 % inferior. For $H/L \neq 1$, the performance increased significantly, especially for small ratios of H/L and a high percentage of cavity area ($\varphi_{1+2} = 95\ \%\varphi_c$) distributed to the cavity branches. Moreover, when compared with a tree-shaped configuration, the results of a double Y-shaped cavity behaved better than the configurations with one and two branches ($N = 1$ and 2) and worse than the cases with three and four branches ($N = 3$ and 4).

In general, results indicated that the increase in complexity benefits the thermal performance of isothermal cavities. This complexity can be obtained by the addition of more freedom to the branches of the cavity, which can be observed from the double T and tree-shaped configuration with $N = 2$ towards the double Y, where the angles of the branches are the new DOFs. Another possibility is the increase in the number of branches, as noticed from double-Y-shaped cavity towards the tree-shaped configuration with $N = 3$. A recent study using wavy-shaped branches [58] obtained thermal performances varying from $\theta_{max} = 0.0163$ for $N = 1$ to $\theta_{max} = 0.0026$ for $N = 4$, corroborating the previous observation about the complexity of the cavities. This study is not more explored here because it is restricted to a geometrical optimization of the cavity, not concerned with the influence of the degrees of freedom over the thermal performance, which is the main purpose in of the present work.

5. Concluding remarks

This work performed a geometrical investigation of a complex cavity (double-Y) with seven DOFs inserted into a rectangular solid body for chilling the domain subject to heat generation. Constructal design is associated with a differential evolution heuristic algorithm to predict the

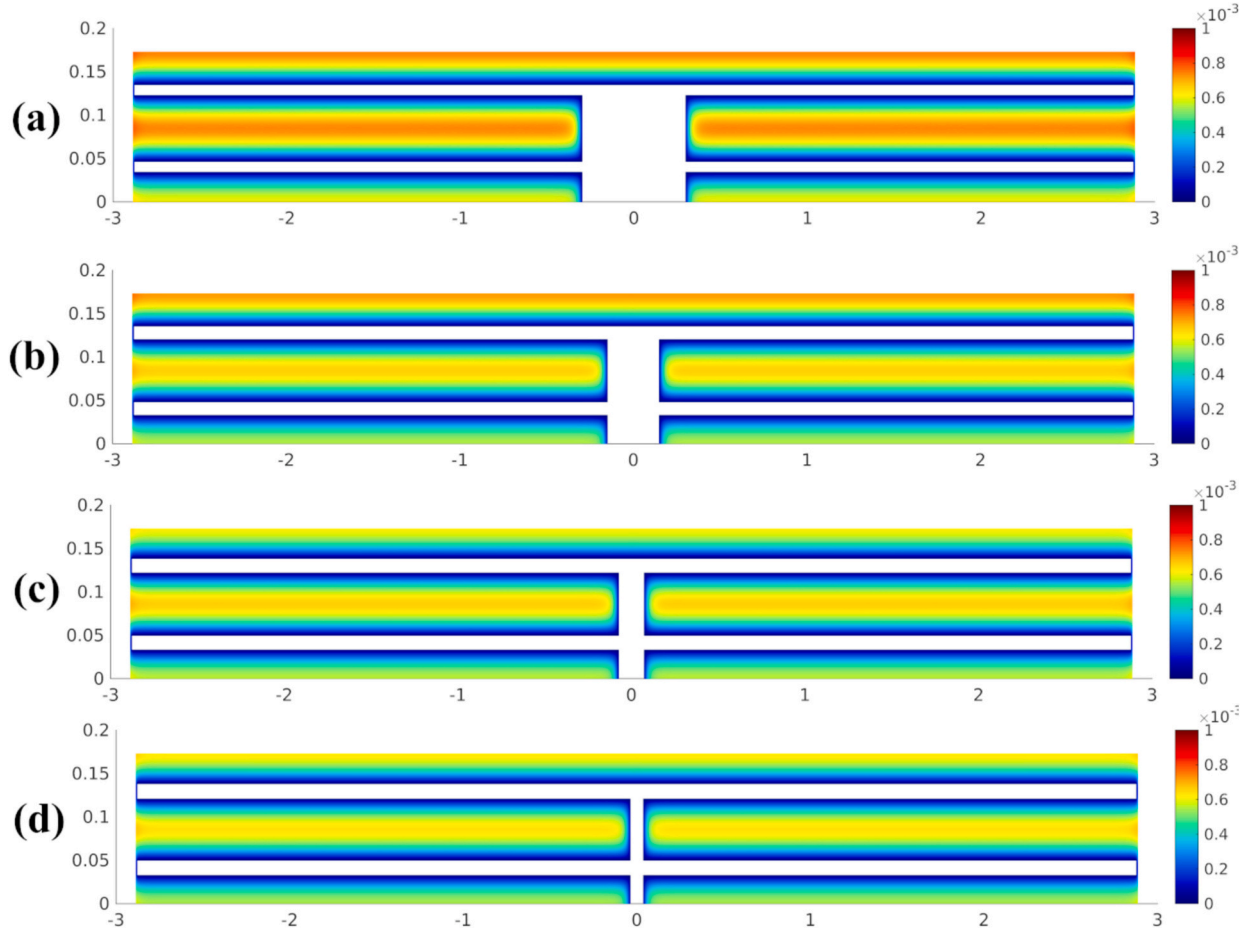

Fig. 14. Optimal geometries for different values of $\varphi_c = 0.2$, $(H/L)_o = 0.03$ $(S_1/H_0)_{3o} = 0.3$, and $(H_2/L_2)_{6o} = (H_1/L_1)_{7o}$, with different area constraint distribution for $\varphi_1 = \varphi_2$: a) $\varphi_2 = 0.03$ (60 %), $(H_0/L_0)_{2o} = 0.2266$, $(H_2/L_2)_{6o} = 45.07\times 10^{-4}$, $(\theta_{max})_{7m} = 7.7 \times 10^{-4}$; b) $\varphi_2 = 0.04$ (80 %), $(H_0/L_0)_{2o} = 0.4566$, $(H_2/L_2)_{6o} = 53.71 \times 10^{-4}$, $(\theta_{max})_{7m} = 7.5 \times 10^{-4}$; c) $\varphi_2 = 0.045$ (90 %), $(H_0/L_0)_{2o} = 0.9566$, $(H_2/L_2)_{6o} = 57.21 \times 10^{-4}$, $(\theta_{max})_{7m} = 6.9 \times 10^{-4}$; d) $\varphi_2 = 0.0475$ (95 %), $(H_0/L_0)_{2o} = 1.9$, $(H_2/L_2)_{6o} = 58.87 \times 10^{-4}$, and $(\theta_{max})_{7m} = 6.7 \times 10^{-4}$.

Table 3
Comparison between the θ_{max} obtained for the cavity with double-Y-shaped configuration and other geometries presented in the literature.

Configuration \ condition	$\varphi_c = 0.1$ and $H/L =$ 1.0	$\varphi_c = 0.1$ and $H/L >$ 1.0	$\varphi_c = 0.1$, H/L < 1.0 and φ_{1+2} $= 60$ %φ_c	$\varphi_c = 0.2$; $\varphi_{1+2} =$ $0.95\varphi_c$
I [28]	0.1008	NA	NA	NA
T [28]	0.0710	NA	NA	NA
H [13]	0.0245	NA	NA	NA
Y [44,45]	0.0611	0.0038	NA	NA
Various I [40]	0.0064	NA	NA	NA
X [29]	0.0330	NA	NA	NA
ψ [30]	0.0180	NA	NA	NA
double T [26]	0.0281	0.0034	9×10^{-4}	NA
Tree [14] – $N = 1$	0.0657	NA	NA	NA
Tree [14] – $N = 2$	0.0241	NA	NA	NA
Tree [14] – $N = 3$	0.0114	NA	NA	NA
Tree [14] – $N = 4$	0.0065	NA	NA	NA
double Y	0.0182	0.0035	8.8×10^{-4}	6.7×10^{-4}

NA – Not Applicable (configuration not studied in the literature).

global optimal configurations to define the points of investigation of the dependent DOF analyzed. The reduction in the computational effort allowed the investigation of the influence of the cavity fraction area (φ_c) over the $(\theta_{max})_{7m}$ and corresponding optimal DOFs. The complex configuration studied here had not been wholly optimized before in the literature.

The results of the present work allowed the achievement of the following conclusions:

- the insertion of the new angles for the bifurcated branches (α and β) in comparison with the double T configuration was beneficial to minimize (θ_{max}) for square solid domains ($H/L = 1.0$), as well as, for the investigated ratio $H/L = 3.77$. Configurations in the form of treelike (similar to that observed, for example, in leaves) increased the number of hot regions of temperature, which improves the performance by homogenization of temperature fields, i.e., following the optimal distribution of imperfections principle;

- for the lowest and highest extremes of H/L, the optimal configurations changed to double-T- and I-cavity configurations, i.e., degenerating the double-Y-cavity configuration into more straightforward configurations. This behavior can be associated with the degeneration of the flow system from volume-to-point to point-to-point configuration and shows the importance of the solid domain constraint over the design of the cavity;

- results obtained for the double-Y-cavity configuration were compared with other shapes previously studied in the literature. It was noticed that, for $H/L = 1.0$, the double-Y-cavity presented a significant improvement in the thermal performance in comparison with several configurations as I-, T-, Y-, X-, H-, various I- and double-T-cavity [13,26,28,40,44,45], for the same thermal conditions, being a possible evolution of these configurations. The double-Y-cavity configuration had a similar performance to the ψ configuration [30] with a difference of 1.0 % and an intermediate performance between $N = 2$ and $N = 3$ for the tree-shaped configuration studied in Hajmohammadi [14];

- results also indicated that the distribution of the area between the trunk and bifurcated branches could have a significant influence over the thermal performance, which was demonstrated by the change in the distribution of $\varphi_{1+2} = 60\ \%\varphi_c$ to $\varphi_{1+2} = 95\ \%\varphi_c$ for $\varphi_c = 0.2$ that allowed to an improvement of nearly 12 % in the thermal performance.

The combination of ES and DE methods applied in this work not only led to the achievement of optimal geometries and allowed the reproduction of DOF effects over thermal performance for a complex geometry with seven degrees of freedom, but also reduced drastically the computational effort. The efficiency of the methodology reassures its potential for future studies of complex branched designs. Moreover, other boundary conditions for the double-Y-cavity can be investigated, showing the influence of the magnitude of the cooling capacity of the cavity (measured by coefficient h) over the design of complex cavities.

CRediT authorship contribution statement

Gill Velleda Gonzales: Visualization, Validation, Software, Investigation, Data curation, Conceptualization. **Cesare Biserni:** Writing – review & editing, Supervision, Resources. **Luiz Alberto Oliveira Rocha:** Writing – original draft, Visualization, Validation, Supervision, Methodology, Investigation, Formal analysis, Data curation, Conceptualization. **Emanuel da Silva Diaz Estrada:** Writing – original draft, Software, Investigation, Formal analysis, Data curation, Conceptualization. **Liércio André Isoldi:** Writing – original draft, Visualization, Validation, Software, Investigation, Formal analysis, Data curation, Conceptualization. **Antônio José da Silva Neto:** Writing – original draft, Validation, Software, Methodology, Investigation, Formal analysis, Data curation, Conceptualization. **Elizaldo Domingues dos Santos:** Writing – original draft, Visualization, Validation, Supervision, Methodology, Investigation, Funding acquisition, Formal analysis, Data curation, Conceptualization.

Declaration of competing interest

The authors declare that they have no known competing financial interests or personal relationships that could have appeared to influence the work reported in this paper.

Acknowledgments

G. V. Gonzales thank IFSul – Instituto Federal Sul-rio-grandense for the authorization of the license to pursue his doctorate degree. Authors L.A.O. Rocha, L.A. Isoldi, A.J. Silva Neto and E.D. dos Santos thank CNPq – National Council of Scientific and Technological Development for the research grant (Processes: 307791/2019-0, 308958/2019-5, 309648/2021-1, 308396/2021-9). Authors also thank FAPERGS – Fundação de Apoio à Pesquisa do Estado do Rio Grande do Sul (Grant number: 19/2551-0001847-9) and FAPERJ – Fundação Carlos Chagas Filho de Amparo à Pesquisa do Estado do Rio de Janeiro (Grant number: E-26/202.878/2017 and E-26/200.899/2021). This study was financed in part by the Coordenação de Aperfeiçoamento de Pessoal de Nível Superior (CAPES) – Finance Code 001. C. Biserni is sponsored by the National Recovery and Resilience Plan (NRRP) of the Italian Ministry of University and Research, "Ecosystem for Sustainable Transition in Emilia-Romagna" (Ecosister), Spoke 4.

Data availability

Data will be made available on request.

References

[1] A. Bejan, Constructal-theory network of conducting paths for cooling a heat generating volume, Int. J. Heat Mass Transf. 40 (1997) 799–816, https://doi.org/10.1016/0017-9310(96)00175-5.
[2] A. Bejan, Shape and Structure, from Engineering to Nature, Cambridge University Press, Cambridge, UK, 2000.
[3] A. Bejan, J. Zane, Design in Nature: How the Constructal Law Governs Evolution in Biology, 1st ed., Doubleday, New York, 2012.
[4] A. Bejan, Freedom and Evolution: Hierarchy in Nature, Society and Science, Springer International Publishing, Cham, Switzerland, 2020.
[5] A. Bejan, The Physics of Life: The Evolution of Everything, St. Martin's Press, New York, 2016.
[6] M. Reis, A.H. Miguel, A.F. Aydin, Constructal theory of flow architecture of the lungs, Med. Phys. 31 (2004) 1135–1140, https://doi.org/10.1118/1.1705443.
[7] A.N. Impiombato, F.S.F. Zinani, L.A.O. Rocha, C. Biserni, Constructal design of an idealize arterial bypass graft: effect of the bypass attachment pointon resistance to flow, J. Appl. Comput. Mech. 7 (2021) 334–344, https://doi.org/10.22055/jacm.2020.35246.2607.
[8] A.H. Reis, Constructal view of the scaling laws of street networks – the dynamics behind geometry, Phys. A: Stat. 387 (2008) 617–622, https://doi.org/10.1016/j.physa.2007.10.003.
[9] A. Bejan, interviewed by A. Kosner, Freedom is good for design, how to use constructal theory to liberate any flow system, Forbes. https://www.forbes.com/sites/anthonykosner/2012/03/18/freedom-is-good-for-design-how-to-use-constructal-theory-to-liberate-any-flow-system, 2012.
[10] L.A.O. Rocha, S. Lorente, A. Bejan, Constructal theory in heat transfer, in: F. A. Kulacki (Ed.), Handbook Thermal Science Engineering, Springer Cham, 2018.
[11] E.D. dos Santos, L.A. Isoldi, M.N. Gomes, L.A.O. Rocha, The constructal design applied to renewable energy systems, in: E. Rincón-Mejía, A. de las Heras (Eds.), Sustainable Energy Technologies, first ed, CRC Press - Taylor & Francis Group, Boca Raton, 2017, pp. 63–87.
[12] L. Chen, H. Feng, Z. Xie, F. Sun, Progress of constructal theory in China over the past decade, Int. J. Heat Mass Transf. 130 (2019) 393–419, https://doi.org/10.1016/j.ijheatmasstransfer.2018.10.064.
[13] C. Biserni, L.A.O. Rocha, G. Stanescu, E. Lorenzini, Constructal H-shaped cavities according to Bejan's theory, Int. J. Heat Mass Transf. 50 (2007) 2132–2138, https://doi.org/10.1016/j.ijheatmasstransfer.2006.11.006.
[14] M.R. Hajmohammadi, Optimal design of tree-shaped inverted fins, Int. J. Heat Mass Transf. 116 (2018) 1352–1360, https://doi.org/10.1016/j.ijheatmasstransfer.2017.09.042.
[15] P.M. Rodrigues, C. Biserni, C.C. de Escobar, L.A.O. Rocha, L.A. Isoldi, E.D. dos Santos, Geometric optimization of a lid-driven cavity with two rectangular intrusions under mixed convection heat transfer: a numerical investigation motivated by constructal design, Int. Commun. Heat Mass Transf. 117 (2020) 104759, https://doi.org/10.1016/j.icheatmasstransfer.2020.104759.
[16] V. Joshi, M.K. Rathod, Constructal enhancement of thermal transport in latent heat storage systems assisted with fins, Int. J. Therm. Sci. 145 (2019) 105984, https://doi.org/10.1016/j.ijthermalsci.2019.105984.
[17] H. Feng, Z. Zhang, L. Chen, Y. Ge, J. Yu, Constructal design for tree-shaped compound heat transfer channel in a disc heat generation body, Int. Commun. Heat Mass Transf. 132 (2022) 105929, https://doi.org/10.1016/j.icheatmasstransfer.2022.105929.
[18] D.O. Ariyo, T. Bello-Ochende, Constructal design of two-phase stacked microchannel heat exchangers for cooling at high heat flux, Int. Commun. Heat Mass Transf. 125 (2021) 105294, https://doi.org/10.1016/j.icheatmasstransfer.2021.105294.
[19] W. Zhang, L. Chen, H. Feng, Y. Ge, Adding branched fin angle as degree-of-freedom improves performance of a T-Y-shaped fin, Case Stud. Therm. Eng. 61 (2024) 105031, https://doi.org/10.1016/j.csite.2024.105031.
[20] X. Liu, H. Feng, L. Chen, Y. Ge, Constructal design of a rectangular porous fin considering minimization of maximum temperature difference and pumping power consumption, Sci. China Technol. Sci. 67 (3) 919–929. doi:https://doi.org/10.1007/s11431-023-2495-y.
[21] X. Liu, H. Feng, L. Chen, Y. Ge, Design of multi-scale cylindrical porous fin based on constructal design, Int. Commun. Heat Mass Transf. 153 (2024) 107352, https://doi.org/10.1016/j.icheatmasstransfer.2024.107352.
[22] B. Wu, H. Feng, L. Chen, Y. Ge, X. Liu, Constructal design of a hybrid heat sink with rectangular microchannel and porous fin in a 3D electronic device with artificial neural-network, NSGA-II and different decision-making methods, Int. Commun. Heat Mass Transf. 158 (2024) 107954, https://doi.org/10.1016/j.icheatmasstransfer.2024.107954.
[23] T. da Silveira, V.T. Pinto, J.P.S. Neufeld, A. Pavlovic, L.A.O. Rocha, E.D. dos Santos, L.A. Isoldi, Applicability evidence of constructal design in structural engineering: case study of biaxial elasto-plastic buckling of square steel plates with elliptical cutout, J. Appl. Comput. Mech. 7 (2021) 922–934, https://doi.org/10.22055/JACM.2021.35385.2647.
[24] J.C. Martins, C. Fragassa, M.M. Goulart, E.D. dos Santos, L.A. Isoldi, M.N. das Gomes, L.A.O. Rocha, Constructal design of an overtopping wave energy converter incorporated in a breakwater, J. Mar. Sci. Eng. 10 (4) (2022) 471, https://doi.org/10.3390/jmse10040471.
[25] W. Wu, L. Chen, F. Sun, On the "area to point" flow problem based on constructal theory, Energy Convers. Manag. 48 (1) (2007) 101–105, https://doi.org/10.1016/j.enconman.2006.05.009.
[26] G.V. Gonzales, G. Lorenzini, L.A. Isoldi, L.A.O. Rocha, E.D. dos Santos, A.J. Silva Neto, Constructal design and simulated annealing applied to the geometric optimization of an isothermal double T-shaped cavity, Int. J. Heat Mass Transf. 174 (2021) 121268, https://doi.org/10.1016/j.ijheatmasstransfer.2021.121268.
[27] X. Zhang, S. Lorente, The growth of capillary networks by branching for maximum fluid access, Sci. Rep. 13 (1) (2023) 11278, https://doi.org/10.1038/s41598-023-38381-6.

[28] C. Biserni, L.A.O. Rocha, A. Bejan, Inverted fins: geometric optimization of the intrusion into a conducting wall, Int. J. Heat Mass Transf. 47 (2004) 2577–2586, https://doi.org/10.1016/j.ijheatmasstransfer.2003.12.018.
[29] G. Lorenzini, C. Biserni, L.A.O. Rocha, Geometric optimization of X-shaped cavities and pathways according to Bejan's theory: comparative analysis, Int. J. Heat Mass Transf. 73 (2014) 1–8, https://doi.org/10.1016/j.ijheatmasstransfer.2014.01.055.
[30] M.R. Hajmohammadi, Introducing a ψ-shaped cavity for cooling a heat generating medium, Int. J. Therm. Sci. 121 (2017) 204–212, https://doi.org/10.1016/j.ijthermalsci.2017.07.010.
[31] S. Zehisaadat, R.K. Khalajzadeh, M.R. Hajmohammadi, G. Lorenzini, Geometric optimization of T-shaped fin and inverted fin based on minimum entropy generation objective, J. Eng. Thermophys. 31 (4) (2022) 668–687, https://doi.org/10.1134/S1810232822040129.
[32] G.V. Gonzales, C. Biserni, E.S.D. da Estrada, G.M. Platt, L.A. Isoldi, L.A.O. Rocha, A. J. Silva Neto, E.D. dos Santos, Investigation on the association of differential evolution and constructal design for geometric optimization of double Y-shaped cooling cavities inserted into walls with heat generation, Appl. Sci. 13 (2023), https://doi.org/10.3390/app13031998.
[33] L. Chen, H. Feng, F. Zhang, Y. Ge, Constructal design for composite heat dissipating structure composed of an "arrow"-shaped high conductivity channel and an externally connected "T"-shaped fin, Int. Commun. Heat Mass Transf. 153 (2024) 107341, https://doi.org/10.1016/j.icheatmasstransfer.2024.107341.
[34] T. Xie, L. Chen, H. Feng, Y. Gee, Constructal design for a composite structure with an "X"-shaped high conductivity channel and a "T"-shaped fin, Int. Commun. Heat Mass Transf. 159 (2024) 107985, https://doi.org/10.1016/j.icheatmasstransfer.2024.107985.
[35] H. Feng, Z. Zhang, L. Chen, Y. Gee, Constructal design for H-shaped compound heat transfer path in a rectangular heat generation body, Int. J. Heat Mass Transf. 225 (2024) 125442, https://doi.org/10.1016/j.ijheatmasstransfer.2024.125442.
[36] H. Zhu, L. Chen, H. Feng, Y. Ge, Constructal design of comb-shaped high thermal conductivity channel in a stacked chip, Int. Commun. Heat Mass Transf. 155 (2024) 107557, https://doi.org/10.1016/j.icheatmasstransfer.2024.107557.
[37] Z.H. Xie, L.G. Chen, F.R. Sun, Constructal optimization on T-shaped cavity based on entransy dissipation minimization, Chin. Sci. Bull. 54 (2009) 4418–4427, https://doi.org/10.1007/s11434-009-0507-6.
[38] Z. Xie, L. Chen, F. Sun, Geometry optimization of T-shaped cavities according to constructal theory, Math. Comput. Model. 52 (2010) 1538–1546, https://doi.org/10.1016/j.mcm.2010.06.017.
[39] G. Lorenzini, C. Biserni, L.A. Isoldi, E.D. dos Santos, L.A.O. Rocha, Constructal design applied to the geometric optimization of Y-shaped cavities embedded in a conducting medium, J. Electron. Packag. 133 (2011) 041008, https://doi.org/10.1115/1.4005296.
[40] M.R. Hajmohammadi, S. Poozesh, A. Campo, S.S. Nourazar, Valuable reconsideration in the constructal design of cavities, Energy Convers. Manag. 66 (2012) 33–40, https://doi.org/10.1016/j.enconman.2012.09.031.
[41] G. Lorenzini, F.L. Garcia, E.D. dos Santos, C. Biserni, L.A.O. Rocha, Constructal design applied to the optimization of complex geometries: T-Y-shaped cavities with two additional lateral intrusions cooled by convection, Int. J. Heat Mass Transf. 55 (2012) 1505–1512, https://doi.org/10.1016/j.ijheatmasstransfer.2011.10.057.
[42] L.A.O. Rocha, G. Lorenzini, C. Biserni, Y. Cho, Constructal design of a cavity cooled by convection, Int. J. Des. Nat. Ecodynam. 5 (2010) 212–220, https://doi.org/10.2495/DNE-V5-N3-212-220.
[43] G. Lorenzini, C. Biserni, F.B. Link, L.A. Isoldi, E.D. dos Santos, L.A.O. Rocha, Constructal design of T-shaped cavity for several convective fluxes imposed at the cavity surfaces, J. Eng. Thermophys. 22 (2013) 309–321, https://doi.org/10.1134/S1810232813040048.
[44] G. Lorenzini, C. Biserni, E.D. Estrada, L.A. Isoldi, E.D. dos Santos, L.A.O. Rocha, Constructal design of convective Y-shaped cavities by means of genetic algorithm, J. Heat Transf. 136 (2014) 071702, https://doi.org/10.1115/1.4027195.
[45] G. Lorenzini, C. Biserni, E.S.D. da Estrada, E.D. dos Santos, L.A. Isoldi, L.A. O. Rocha, Genetic algorithm applied to geometric optimization of isothermal Y-shaped cavities, J. Electron. Packag. 136 (2014) 031011, https://doi.org/10.1115/1.4027421.
[46] G.V. Gonzales, E.S.D. da Estrada, L.R. Emmendorfer, L.A. Isoldi, G. Xie, L.A. O. Rocha, E.D. dos Santos, A comparison of simulated annealing schedules for constructal design of complex cavities intruded into conductive walls with internal heat generation, Energy 93 (2015) 372–382, https://doi.org/10.1016/J.ENERGY.2015.09.058.
[47] G.V. Gonzales, E.D. dos Santos, L.A. Isoldi, L.A.O. Rocha, A.J. Silva Neto, W. R. Telles, Constructal design of double-T shaped cavity with stochastic methods Luus-Jaakola and simulated annealing, Defect Diffus. Forum 370 (2017), https://doi.org/10.4028/www.scientific.net/DDF.370.152.
[48] G.V. Gonzales, L.A. Isoldi, L.A.O. Rocha, A.J. da Silva Neto, E.D. dos Santos, Evaluation of a differential evolution/constructal design algorithm for geometrical optimization of double T-shaped cavity intruded into a heat generating wall, Defect Diffus. Forum 396 (2019) 145–154, https://doi.org/10.4028/www.scientific.net/DDF.396.145.
[49] T.M. Fagundes, G. Lorenzini, E.S.D. da Estrada, L.A. Isoldi, E.D. dos Santos, L.A. O. Rocha, A.J. da Silva Neto, Constructal design of conductive asymmetric tri-forked pathways, J. Eng. Thermophys. 28 (2019) 26–42, https://doi.org/10.1134/S181023281901003X.
[50] A. Samanta, S. Sarkar, R. Das, H. Mondal, Machine learning algorithms on predicting the turbulent mixed convection flow in a driven-cavity with two horizontal cylinders, Int. Commun. Heat Mass Transf. 159 (2024) 108064, https://doi.org/10.1016/j.icheatmasstransfer.2024.108064.
[51] M. Boyareh, M. Baghoolizadeh, An overview of the magnetic field effect on heat transfer and entropy generation in cavities: application of the second law of thermodynamics and artificial intelligence, Int. Commun. Heat Mass Transf. 151 (2024) 107238, https://doi.org/10.1016/j.icheatmasstransfer.2023.107238.
[52] U.G. Matlab, T.M. Inc, Partial Differential Equation Toolbox™ User's Guide R2018b, Natick. https://la.mathworks.com/help/pdf_doc/pde/pde.pdf, 2018.
[53] S. Cabezas, G. Hegedűs, P. Bencs, Thermal experimental and numerical heat transfer analysis of a solid cylinder in longitudinal direction, Anal. Tech. Szeged. 17 (1) (2023) 16–27, https://doi.org/10.14232/analecta.2023.1.16-27.
[54] S.W. Churchill, H.H.S. Chu, Correlating equations for laminar and turbulent free convection from a vertical plate, Int. J. Heat Mass Transf. 18 (1975) 1323–1329.
[55] P. Siarry, Metaheuristics, 2016, https://doi.org/10.1007/978-3-319-45403-0.
[56] U.K. Chakraborty, Advances in Differential Evolution, Springer Berlin Heidelberg, St. Louis, 2008, https://doi.org/10.1007/978-3-540-68830-3.
[57] R. Storn, K. Price, Differential evolution - a simple and efficient heuristic for global optimization over continuous spaces, J. Glob. Optim. 11 (1997) 341–359.
[58] C.H. Huang, P.-W. Tung, A shape design problem in determining the optimal geometry of wavy-shaped inverted fins, Inverse Probl. Sci. Eng. 28 (2020) 716–738, https://doi.org/10.1080/17415977.2019.1683175.